Contrib Mineral Petrol (1999) 135: 133–150

Andrea Marzoli · Paul R. Renne · Enzo M. Piccirillo
Castorina Francesca · Giuliano Bellieni
Adolpho J. Melfi · Jean B. Nyobe · Jean N'ni

Silicic magmas from the continental Cameroon Volcanic Line (Oku, Bambouto and Ngaoundere): ^{40}Ar-^{39}Ar dates, petrology, Sr-Nd-O isotopes and their petrogenetic significance

Received: 24 February 1998 / Accepted: 22 September 1998

Abstract The intraplate Cameroon Volcanic Line (CVL) straddles the African-South Atlantic continent-ocean boundary and is composed mainly of alkaline basic volcanic rocks. Voluminous silicic volcanics characterize the continental sector of the CVL. We present here new geochemical, isotopic (Sr-Nd-O) and $^{40}Ar/^{39}Ar$ geochronological data on the main silicic volcanic centres of the Western (Mt. Oku, Sabga and Mt. Bambouto) and Eastern (Ngaoundere plateau) Cameroon Highlands. The silicic volcanism of Mt. Oku, Sabga and Mt. Bambouto occurred between 25 and 15 Ma and is represented by voluminous quartz-normative trachytes and minor rhyolitic ignimbrites. At Mt. Bambouto central volcano about 700 m of silicic volcanics erupted in less than 2.7 million years. These silicic volcanics are associated with slightly to moderately alkaline basalts and minor basanites. In general, onset of the silicic volcanism migrated from NE (Oku: 25 Ma) to SW (Sabga: 23 Ma; Bambouto: 18 Ma; and Mt. Manengouba: 12 Ma). The silicic volcanism of the Ngaoundere plateau (eastern branch of the CVL) is instead dominated by nepheline-normative trachytes which are associated with strongly alkaline basalts and basanitic rocks. These Ne-trachytes are younger (11-9 Ma) than the Q-trachytes of the Western Highlands. The least differentiated silicic volcanics are isotopically similar ($^{87}Sr/^{86}Sr < 0.70380$; $^{143}Nd/^{144}Nd > 0.51278$) to the associated alkaline basalts suggesting differentiation processes without appreciable interaction with crustal materials. Such interactions may, however, have played some role in the genesis of the most evolved silicic volcanics which have $^{87}Sr/^{86}Sr$ as high as 0.705–0.714. Fractional crystallization is the preferred mechanism for genesis of the silicic melts of both Western and Eastern Highlands, as shown by modeling major and trace element variations. The genesis of the least evolved Q-trachytes from the Western Highlands, starting from slightly to moderately alkaline basalts, is compatible with fractionation of dominantly plagioclase, clinopyroxene and magnetite. Crystal fractionation may have occurred at low pressure and at QFM buffer f_{O_2}conditions. Parental magmas of the Ngaoundere Ne-trachytes are likely instead to have been strongly alkaline basalts which evolved through crystal fractionation at higher P (6-2 kbar) and f_{O_2} (QFM + 2). The migration (25 to 12 Ma) of the silicic volcanism from NE to SW in the continental sector of the CVL is reminiscent of that (31-5 Ma) of the onset of the basic volcanism in the oceanic sector (Principe to Pagalu islands) of the CVL. These ages, and that (11-9 Ma) of the silicic volcanism of the Ngaoundere plateau, indicate that the Cameroon Volcanic Line as a whole may not be easily interpreted as the surface expression of hot-spot magmatism.

A. Marzoli (✉) · E.M. Piccirillo
Dipartimento di Scienze della Terra, Università Trieste,
Via E. Weiss 8, I-34127 Trieste, Italy
Fax: #39.40.6762213, Tel.: #39.40.6762222
e-mail: marzoli@univ.trieste.it

A. Marzoli · P.R. Renne
Berkeley Geochronology Center, 2455 Ridge Road,
94709 Berkeley, CA, USA

F. Castorina
Dipartimento di Scienze della Terra, Università La Sapienza,
P.le A. Moro, 00185 Roma, Italy

G. Bellieni
Dipartimento di Mineralogia e Petrologia, Università Padova,
Corso Garibaldi 37, 35100 Padova, Italy

A.J. Melfi
Instituto Astronômico e Geofísico,
Universidade de São Paulo,
C.P. 9638, 0165-970 São Paulo, Brazil

J.B. Nyobe
Ministere de Recherche Scientifique Technologique,
Yaoundè, Cameroon

J. N'ni
Institute de Recherche Geologique Minerarie, Buea, Cameroon

Editorial responsibility: T.L. Grove

Introduction

Alkaline basic igneous rocks and SiO_2-oversaturated silicic volcanic rocks often characterize intraplate geo-

tectonic setting (e.g. Kampunzu and Lubala 1991; Landoll et al. 1994; Wilson et al. 1995; Panter et al. 1997). The petrogenetic aspects (e.g. fractional crystallization, interaction with crustal materials, melting processes of lower crust/underplated igneous rocks), which may explain the relationships between alkaline basalts and the associated silicic rocks, are still debated. A possible explanation that SiO_2-oversaturation can be achieved through interaction with siliceous crustal material(s) seems reasonable where alkaline basic basalts are associated with SiO_2-oversaturated rocks whose Sr-Nd-O isotopic compositions and their major and trace elements indicate a distinct crustal signature (e.g. Foland et al. 1993; Landoll et al. 1994; Wilson et al. 1995; Brotzu et al. 1997).

The role of crustal contamination and the genetic relationships between alkaline basalts and quartz (Q) and nepheline (Ne) normative trachytes can be examined in the Cameroon Volcanic Line (CVL) where several volcanic complexes (Fig. 1) are composed of basic alkaline igneous rocks and Q and Ne-normative differentiated rocks (Fitton and Dunlop 1985; Fitton 1987; Nono et al. 1994; Marzoli 1996). The CVL is Cenozoic (42 Ma) to Quaternary in age and extends (Fig. 1) from the interior of the West African continent to the oceanic islands in the Gulf of Guinea, straddling the continent-ocean boundary. Despite the general similarity of the chemistry and Sr-Nd isotopic compositions of the basic volcanics all along the CVL (Fitton and Dunlop 1985; Deruelle et al. 1991), the differentiated volcanic rocks of the oceanic and continental sectors are compositionally distinct (Fig. 2). The former are mainly represented by phonolitic rocks, while the latter are dominated by voluminous Q-trachytes (Fitton 1987; Halliday et al. 1988; Marzoli 1996). This suggests that crustal contamination has to be considered, particularly in the genesis of the continental CVL Q-trachytes (cf. Fitton 1987).

A detailed and precise knowledge of the ages of the continental CVL volcanics is still lacking. The few K/Ar (Dunlop 1983; Fitton and Dunlop 1985; Fitton 1987 and references therein) and $^{40}Ar/^{39}Ar$ ages (Lee et al. 1994a,b; Marzoli 1996) from these volcanics, mainly basalts, show that the activity of the central volcanoes lasted up to 42 million years. In general, CVL silicic volcanics are difficult to date by whole rock K/Ar or $^{40}Ar/^{39}Ar$ because of their fine-grained groundmass and alteration. Therefore, whole-rock age uncertainty and generally high Rb/Sr ratios (up to 32) in most of the continental CVL silicic volcanics do not allow determination of precise $^{87}Sr/^{86}Sr$ initial isotopic ratios.

The present paper provides nine $^{40}Ar/^{39}Ar$ new feldspar ages of volcanics from the continental sector of CVL (Mts. Bambouto and Oku, and Ngaoundere plateau) and aims at investigating the petrogenesis of the CVL silicic volcanics and the relationships with associated alkaline basalts. It will be shown that crustal contamination is not essential to account for the genesis of SiO_2-oversaturated trachytic magmas, starting from slightly to moderately alkaline basalts.

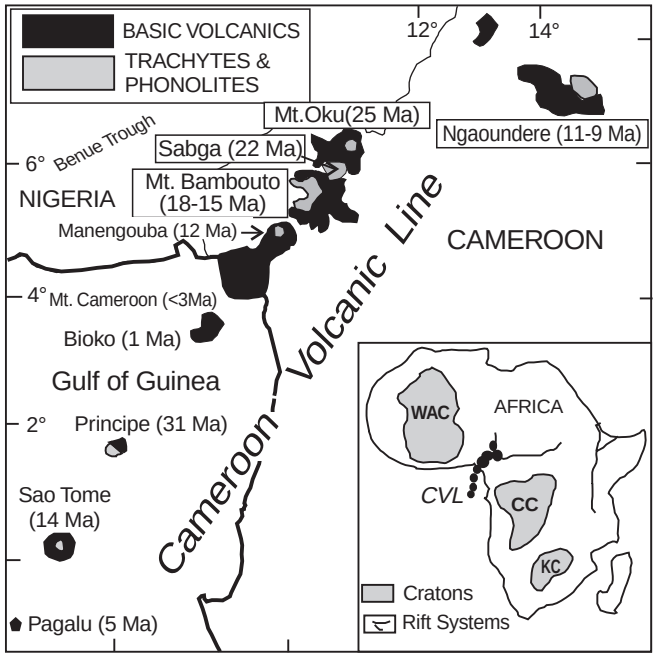

Fig. 1 Sketch map of the central portion of the Cameroon Volcanic Line in West Equatorial Africa (see *inset*). $^{40}Ar/^{39}Ar$ ages of the onset of the silicic volcanism in the continental sector, including K/Ar age of Mt. Manengouba silicic volcanics (Dunlop 1983), and those of the onset of the basic volcanism in the oceanic sector (K/Ar and $^{40}Ar/^{39}Ar$ dates; Fitton and Dunlop 1985; Lee et al. 1994a) are shown. *WAC*, *CC*, and *KC* in the *inset* are the West African, Congo and Kalahari cratons, respectively

Geological outline

The silicic lava flows and ignimbrites investigated in this study belong to the volcanic centres of the Western (Mt. Oku, Sabga area and Mt. Bambouto) and Eastern

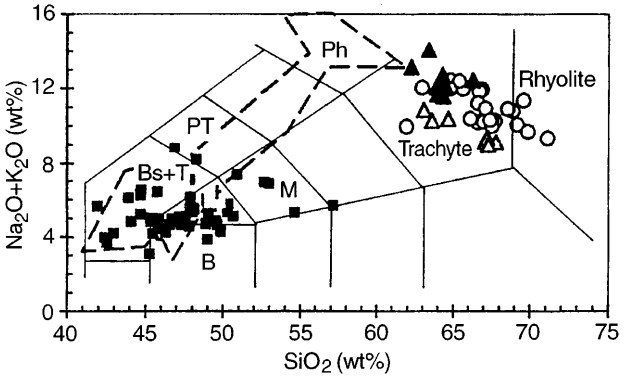

Fig. 2 Total Alkali-Silica classification diagram (LeBas et al. 1986) for continental CVL volcanics: CVL continental basalts *filled squares*, Ngaoundere (Ne-trachytes) *filled triangles*, Mt. Bambouto, Oku and Santa *open circles*, Fongo Tongo and Bandjoun *open triangles*. *Dashed field*: oceanic CVL volcanics (Fitton 1987; Lee et al. 1994a). *B* basalts, *Bs + T* basanites and tephrites, *H* hawaiites, *M* mugearites, *PT* phonotephrites, *Ph* phonolites

(Ngaoundere plateau) Cameroon highlands (Fig. 1), WCH and ECH, respectively.

Geophysical data indicate that in the Ngaoundere region crust and lithosphere are thinned (ca. 20–25 and 80–100 km, respectively; Fairhead and Okereke 1990; Plomerova et al. 1993; Poudjom Djomani et al. 1995, 1997). No evidence of such crustal and lithospheric thinning was detected (Fairhead and Okereke 1987; Poudjom Djomani et al. 1995) in the WCH (Bambouto-Sabga-Oku regions).

The central volcanoes of Mt. Oku and Mt. Bambouto are characterized by collapse calderas. The well preserved caldera of Mt. Bambouto is quite large (ca. 10 km in diameter) and was the site of Quaternary magmatic activity which will be discussed elsewhere. The pre-caldera silicic volcanic activity of Mt. Bambouto is represented by Q-trachytic lava flows, underlain and sometimes covered by minor rhyolitic ignimbrites that may rest directly on the Pan-African granites of the basement (southern slopes: Fig. 3) or on basaltic lava flows (northern slopes). In general, the silicic volcanism was preceded by widespread basalt activity. Small Q-trachytic and rhyolitic lava flows, e.g. Fongo Tongo and Bandjoun (SE of Mt. Bambouto) represent peripheral volcanic activity. A volcanic sequence similar to that of Mt. Bambouto was found at Mt. Oku central volcano. At Sabga Pass, located between Mt. Oku and Mt. Bambouto, the widespread and relatively thick (up to 300 m) silicic volcanics (mainly Q-trachytes) are related to volcanic centres now deeply eroded. In summary, field observations (and petrological and radiometric data, see sections below) revealed that in the investigated Western Cameroon highlands the volcanic activity started with the extrusion of alkaline basalts, and continued with voluminous silicic volcanics, scarce rhyolitic ignimbrites followed by voluminous Q-trachytic lava flows, and rare rhyolitic ignimbrites at the top of the sequence.

The volcanic activity of the Ngaoundere plateau is characterized by strongly to moderately alkaline basic flows, followed by Ne- and scarce Q-trachytic lava flows (cf. Nono et al. 1994). We sampled trachytic flows East of the Ngaoundere town and SW of the Tchabal Nganha volcano studied in detail by Nono et al. (1994). As for the Western Cameroon highlands, Pan-African granitic rocks mainly constitute the crystalline basement of the Ngaoundere plateau.

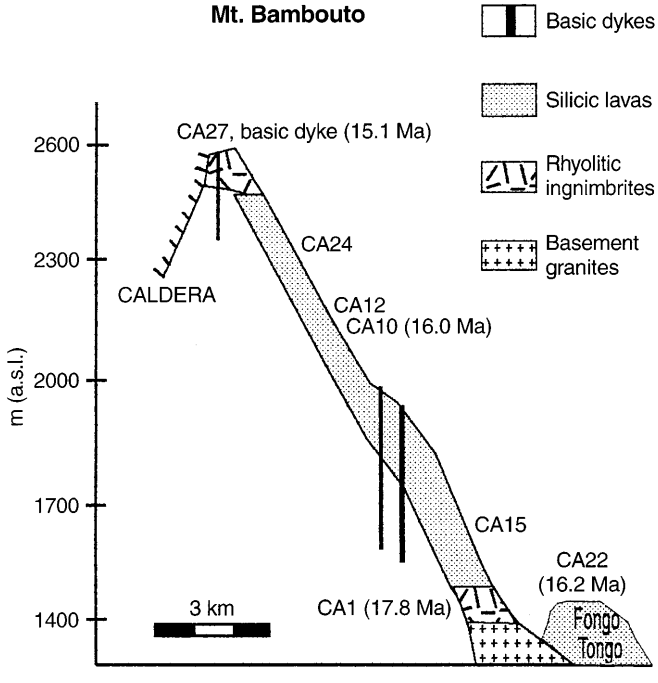

Fig. 3 Sketch of Mt. Bambouto volcanic sequence recorded from its southern slopes, from close to the town of Dschang, to the caldera rim. The approximate sampling height (m a.s.l.) and the $^{40}Ar/^{39}Ar$ age of silicic volcanics are shown. The horizontal scale is indicative

Analytical methods

Fifty-two samples were analyzed for major and trace elements at the Dipartimento di Scienze della Terra, Trieste (Italy), by using a PW 1404 XRF spectrometer and the procedures of Philips (X40 Software Operational Manual, 1994) for the correction of the matrix effects. The analytical uncertainties are less than 5 and 10% for major and trace elements, respectively. FeO was measured by titration and loss on ignition (L.O.I.), corrected for Fe oxidation, by gravimetry. Mineral compositions were determined by a CAMECA-CAMEBAX electron microprobe at the Dipartimento di Mineralogia e Petrologia, Padova (Italy). Results are considered accurate to within 2–3% for major and 10% for minor elements. Rare earth elements (REE) were determined by ICP-MS at the Centre de Recherches Petrographiques et Geochimiques, CNRS, Vandouvre (France) using methods of Govindaraju and Mevelle (1987).

Samples for Sr-Nd isotopic analyses were first dissolved in a HF, HNO_3 and HCl mixture in teflon vials, followed by Sr and Nd collection by ion exchange and reversed-phase chromatography, respectively. The isotopic compositions were measured using a Finnigan MAT 262-RPQ mass spectrometer at the Centro di Studio per il Quaternario e l'Evoluzione Ambientale, CNR, Rome (Italy). Repeated analyses of NBS 987 and La Jolla standards gave average values of 0.71226(2) and 0.511857(8). The reported uncertainties on the Sr-Nd isotopic compositions are at the 2σ confidence level. A few samples were re-analyzed after HCl (6 N) leaching, in order to test the possible effects of alteration. No effects on the measured isotopic compositions were detected.

Samples for oxygen isotopic compositions were analyzed following the procedures of Iacumin et al. (1991). The reported uncertainties are here considered at the 2σ confidence level, and all results are reported as $\delta^{18}O$ per mil, relative to the V-SMOW isotopic standard.

Plagioclase and alkali-feldspar (sanidine) separates were analyzed at the Berkeley Geochronology Center (USA) for $^{40}Ar/^{39}Ar$ ages. Feldspars were hand picked in order to avoid altered or inclusion-bearing crystals and were irradiated for 7 h in the Triga reactor at Oregon State University, along with Fish Canyon sanidine (FCs) neutron fluence monitors. Coarse sanidine crystals (7–15 for each sample) were individually analyzed by total fusion with a NdYAG laser for six of the analyzed samples. Three feldspar separates were step heated using either a defocused laser beam or furnace heating. Ar isotopic compositions were measured in static mode by a MAP215-50 spectrometer, using the procedure described by Renne (1995). Apparent ages were calculated assuming an age of 27.84 Ma for the FCs. Errors are reported at the 2σ level, and do not include uncertainty in the age of FCs or the ^{40}K decay constants.

Table 1 Representative $^{40}Ar/^{39}Ar$ isotopic and geochronology data from single sanidine total fusion (CA179, CA224, CA152) and sanidine laser step heating (CA1). 1σ errors are shown. $^{40}Ar^*$ = radiogenic ^{40}Ar. Isotopic data are corrected for mass discrimination, background, and radioactive decay. The J value is 1.27 E-03 for all analyses

^{40}Ar moles	$^{40}Ar/^{39}Ar$	$^{38}Ar/^{39}Ar$	$^{37}Ar/^{39}Ar$	$^{34}Ar/^{39}Ar$	$^{40}Ar^*/^{39}Ar$	$\%^{40}Ar^*$	Age (Ma)	1σ (Ma)
CAl (Mt. Bambouto)								
2.85E−14	37.836	3.10E−02	1.25E−01	1.03E−01	7.563	20.0	17.272	0.0354
3.36E−14	10.580	1.41E−02	1.17E−01	9.11E−03	7.898	74.6	18.034	0.053
2.56E−14	8.758	1.29E−02	8.83E−02	2.97E−03	7.888	90.1	18.011	0.051
2.93E−14	8.272	1.29E−02	6.91E−02	1.38E−03	7.871	95.1	17.972	0.045
3.01E−14	8.122	1.25E−02	5.46E−02	8.54E−04	7.875	96.9	17.980	0.041
2.70E−14	8.041	1.23E−02	4.76E−02	8.82E−04	7.784	96.8	17.775	0.044
3.19E−14	8.339	1.26E−02	4.48E−02	1.86E−03	7.794	93.5	17.798	0.043
3.39E−14	8.106	1.25E−02	4.42E−02	1.04E−03	7.801	96.2	17.814	0.039
5.17E−14	8.082	1.25E−02	4.12E−02	8.09E−04	7.846	97.1	17.915	0.033
4.95E−14	8.132	1.25E−02	3.91E−02	9.91E−04	7.843	96.4	17.908	0.031
1.43E−14	8.069	1.20E−02	3.75E−02	5.92E−04	7.897	97.9	18.031	0.066
2.03E−14	8.018	1.25E −02	3.93E−02	5.90E−04	7.846	97.9	17.916	0.053
5.79E−14	5.729	8.41E−02	3.62E−02	−6.84E−03	7.755	100.0	17.708	1.048
4.75E−14	7.629	1.18E−02	3.32E−02	−3.14E−06	7.633	100.0	17.431	0.186
3.09E−14	8.073	1.23E−02	4.02E−02	8.85E−04	7.814	96.8	17.843	0.037
8.13E−14	8.061	1.21E−02	3.33E−01	8.18E−04	7.822	97.0	17.860	0.101
1.59E−14	8.057	1.24E−02	4.59E−02	7.80E−04	7.830	97.2	17.879	0.056
1.02E−14	8.084	1.21E−02	5.16E−02	1.05E−03	7.778	96.2	17.762	0.082
4.09E−14	8.067	1.25E−02	4.33E−02	7.73E−07	7.842	97.2	17.905	0.034
2.46E−14	8.043	1.70E−02	2.30E−02	1.21E−03	7.687	95.6	17.554	0.319
6.51E−14	8.057	1.12E−02	4.99E−03	5.45E−07	7.896	98.0	18.029	1.152
CA179 (Sabga)								
7.91E−14	10.549	1.26E−02	4.80E−03	1.79E−03	10.019	95.0	22.847	0.036
5.41E−14	10.463	1.25E−02	4.54E−03	1.59E−03	9.994	95.5	22.790	0.042
5.55E−14	10.542	1.28E−02	4.19E−03	1.95E−03	9.967	94.5	22.728	0.042
4.47E−14	10.449	1.28E−02	5.12E−03	1.68E−03	9.951	95.2	22.693	0.046
8.65E−14	10.664	1.27E−02	4.50E−03	2.41E−03	9.951	93.3	22.691	0.036
7.36E−14	10.234	1.23E−02	3.99E−03	7.65E−03	10.008	97.8	22.820	0.037
7.79E−14	10.094	1.22E−02	5.05E−03	5.32E−03	9.937	98.4	22.659	0.036
CA224 (Mt. Oku)								
3.43E−14	9.048	1.26E−02	6.74E−03	3.32E−03	8.060	89.2	24.781	0.208
3.05E−14	8.561	1.24E−02	1.13E−02	1.56E−03	8.091	94.6	24.875	0.217
4.24E−14	9.251	1.41E−02	1.03E−01	3.69E−03	8.161	88.3	25.091	0.291
6.92E−14	19.225	1.94E−02	1.52E−02	3.76E−02	8.113	42.2	24.943	0.386
2.35E−14	8.532	1.29E−02	1.82E−02	1.41E−03	8.109	95.1	24.931	0.268
9.05E−15	9.144	1.37E−02	2.96E−02	4.24E−03	7.886	86.3	24.250	0.708
3.67E−14	8.545	1.26E−02	5.51E−03	1.52E−03	8.087	94.7	24.864	0.177
8.01E−14	9.684	1.34E−02	7.09E−03	5.14E−03	8.157	84.3	25.077	0.117
3.34E−14	8.390	1.25E−02	1.80E−02	6.99E−04	8.177	97.6	25.138	0.193
1.69E−14	8.380	1.24E−02	8.68E−03	7.74E−04	8.144	97.3	25.037	0.364
1.96E−14	11.333	1.40E−02	1.20E−02	1.12E−02	8.004	70.7	24.609	0.440
1.30E−14	8.723	1.22E−02	2.74E−03	1.90E−03	8.153	93.6	24.064	0.493
1.30E−14	8.839	1.21E−02	3.80E−02	2.32E−03	8.149	92.3	25.051	0.498
4.99E−14	8.294	1.21E−02	6.39E−03	6.08E−04	8.107	97.8	24.924	0.138
2.44E−14	9.444	1.35E−02	1.12E−02	4.42E−03	8.132	86.2	25.0	0.297
CA152 (Ngaoundere)								
5.78E−14	5.085	1.24E−02	1.96E−02	3.72E−04	4.976	97.9	11.383	0.018
7.56E−14	5.070	1.23E−02	2.86E−02	3.02E−04	4.982	98.3	11.397	0.016
7.14E−14	5.034	1.24E−02	4.74E−02	2.05E−04	4.978	98.9	11.386	0.017
3.43E−14	5.062	1.25E−02	2.03E−02	3.22E−04	4.969	98.2	11.366	0.026
3.67E−14	5.129	1.25E−02	6.54E−02	5.38E−04	4.975	97.0	11.381	0.024
7.31E−14	5.889	1.29E−02	4.43E−02	3.09E−04	4.980	84.6	11.392	0.022
5.05E−14	5.026	1.23E−02	2.90E−02	1.83E−04	4.975	99.0	11.379	0.019

$^{40}Ar/^{39}Ar$ ages

$^{40}Ar/^{39}Ar$ dates (Table 1; Fig. 4) mainly concern trachytic lava flows from Mt. Oku (1 Q-trachyte), Sabga (2 Q-trachytes), Mt. Bambouto (1 rhyolitic ignimbrite, 1 Q-trachyte and 1 basalt dyke), Fongo Tongo (1 Q-trachyte) and Ngaoundere plateau (2 Ne-trachytes).

The oldest (24.79 ± 0.11 Ma) trachytic volcanism in the Western Cameroon highlands occurred at Mt. Oku. Proceeding towards the SW, the silicic volcanism be-

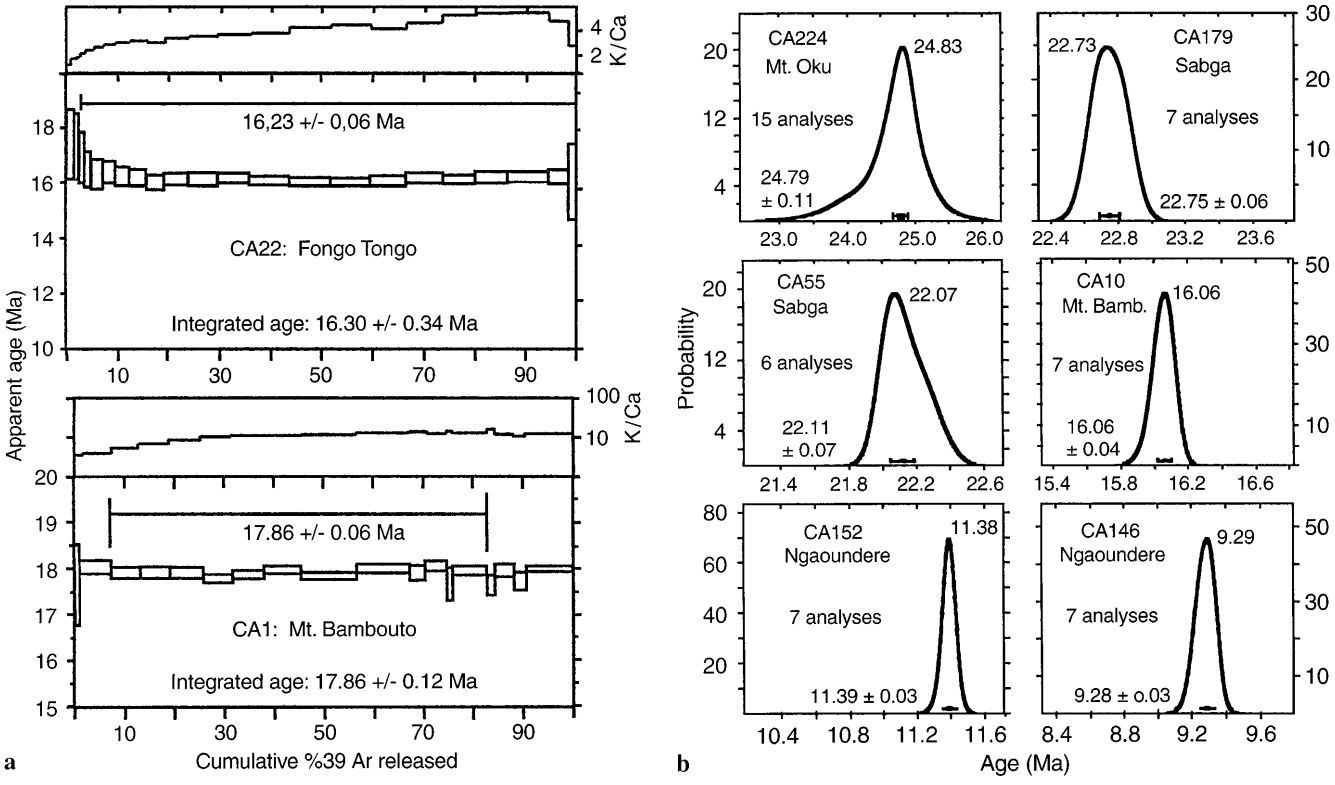

Fig. 4a, b $^{40}Ar/^{39}Ar$ plateau ages (4a), and ideograms (4b) of feldspar separates of silicic volcanics of the CVL. Age uncertainties are at the 2σ level. For CA55 we omitted from the ideogram one analysis that is slightly younger than the other ages (21.83 ± 0.06 Ma; cf. Table 1). It should be noted that this affects the obtained mean age by just 0.2 Ma

comes younger, i.e. Sabga (22.75 ± 0.06 to 22.07 ± 0.07 Ma) and Mt. Bambouto (17.86 ± 0.06 to 15.08 ± 0.05 Ma, see following paragraphs). The age of the dated Fongo Tongo peripheral Q-trachyte (CA22) is 16.23 ± 0.06. Notably, a small rhyolitic plug near Mt. Manengouba, SW of Mt. Bambouto (Fig. 1) was dated at 11.8 Ma (K/Ar age; Dunlop, 1983).

The dated silicic samples from Mt. Bambouto were collected at the bottom of the rhyolitic ignimbrite (ca. 400 m a.s.l., CA1: 17.86 ± 0.06 Ma) and at mid elevation (ca. 2200 m a.s.l., Q-trachyte CA10: 16.06 ± 0.04 Ma) of the volcanic sequence (Fig. 3). A basaltic dyke (ca. 2500 m a.s.l., CA27) intruding Q-trachytic lava flows and the rhyolitic ignimbrites outcropping at the top of the shield was dated at 15.08 ± 0.05 Ma. The ages are consistently younger upwards in the volcanic sequence and indicate that the duration of silicic volcanism of Mt. Bambouto was less than 2.7 million years.

The silicic volcanism on the Ngaoundere plateau (Eastern Cameroon highlands) is dominated by Ne-trachytes. These trachytes, CA152 and CA146, dated at 11.39 ± 0.03 and 9.28 ± 0.03 Ma, respectively, are distinctly younger than the Q-trachytes of the Western Cameroon highlands.

Classification and petrography

Most of the samples investigated are chemically (Table 2) and optically fresh. Altered samples (L.O.I. > 3 wt% and/or with normative corundum) were not considered in this study.

According to the TAS diagram (LeBas et al. 1986), most samples correspond to trachytes, while ca. 15% plot in the rhyolite field (Fig. 2). On a CIPW-normative basis, the trachytes can be distinguished as either nepheline (Ne) and quartz (Q) types. The term peralkaline was used for samples having molar $[(Na_2O + K_2O)/Al_2O_3] > 1.0$. Following Macdonald (1974), peralkaline silicic rocks correspond to comenditic trachytes and comendites, while the chemical characteristics of pantelleritic rocks are shown only by two samples.

All the analyzed silicic volcanics are porphyritic (< 5–10 vol.% phenocrysts) or aphyric. Only CA10 is strongly alkali-feldspar phyric. The groundmass is generally hypohyaline to holocrystalline, often with a trachytic texture. Representative mineral compositions of the silicic volcanics are given in Table 3.

Metaluminous Q-trachytes and rhyolites (Bandjoun) generally contain phenocrysts of plagioclase ($An_{27}Ab_{61}$-$An_{25}Ab_{62}$), alkali-felsdpar ($Or_{52}Ab_{42}$-$Or_{34}Ab_{54}$), Fe-augite to Fe-hedenbergite (rarely augite, e.g. CA55), and rare Ti-magnetites (ulvöspinel = 42–52%). Notably, a crystallographic and crystallochemical study of clinopyroxenes of CVL basic and silicic volcanics supports the cogenetic origin of slightly alkaline basalts and Q-

Table 2 Major (wt%) and trace (ppm) elements (XRF) and rare earth elements (ppm), (ICP-MS, except those superscripted (A): XRF) and some normative parameters (quartz, nepheline, acmite) of representative silicic volcanics, and of basic volcanics and a basement granite sample (CA18) used in the petrogenetic modeling (*Q-Tr* Q-trachytes, *Ne-Tr* Ne-trachytes, *Rhy*. rhyolite, *Alk.Bas*. alkaline basalt, *Haw*. hawaiite, *Mug*. mugearite, *F.To*. Fongo Tongo, *Bandj*. Bandjoun, *Bamb*. Mt. Bambouto, *Nga*. Ngaoundere plateau, *cn* Chondrite-normalized (Boynton 1984), *A.I*. agpaicity index)

Sample	CA23	CA21	CA65	CA9	CA10	CA15	CA24	CA12	CA59	CA176	CA180	CA223	CA152	CA146	CA138	CA40	CA38	CA172	CA133	CA18
Rock-type	Q-Tr.	Q-Tr.	Rhy.	Q-Tr.	Q-Tr.	Q-Tr.	Q-Tr.	Rhy.	Q-Tr.	Q-Tr.	Q-Tr.	Rhy.	No-Tr.	No-Tr.	Q-Tr.	Alk.Bas.	Haw	Mug.	Haw	Granite
Area	F.To.	F.To.	Bandj.	Bamb.	Bamb.	Bamb.	Bamb.	Bamb.	Sabga	Sabga	Oku	Oku	Nga.	Nga.	Nga.	Bamb.	Bamb.	Oku	Nga	Base-ment
SiO_2	63.04	63.58	67.09	62.97	63.69	65.37	68.87	71.15	67.41	63.45	66.74	73.16	62.21	64.29	63.91	47.32	48.97	53.20	48.95	67.97
TiO_2	0.54	0.48	0.36	0.87	1.22	0.78	0.86	1.06	0.47	1.00	0.64	0.54	0.57	0.43	0.43	2.87	2.95	2.25	2.55	0.71
Al_2O_3	15.90	15.51	14.61	15.97	17.21	15.62	12.70	13.13	14.07	16.25	12.88	10.31	18.93	17.74	17.28	15.27	18.14	16.75	16.00	15.30
FeO_t	7.13	7.49	6.31	6.10	5.28	4.80	5.92	5.11	6.37	6.39	8.34	7.24	2.88	3.05	4.38	11.28	11.19	10.75	9.97	3.72
MnO	0.27	0.20	0.12	0.40	0.30	0.19	0.23	0.01	0.31	0.23	0.57	0.40	0.22	0.28	0.30	0.18	0.20	0.22	0.23	0.03
MgO	0.20	0.15	0.05	0.66	0.07	0.40	0.35	0.06	0.11	0.07	0.12	0.10	0.39	0.42	0.78	7.53	3.58	2.98	6.47	0.86
CaO	1.92	2.17	2.21	0.92	0.55	0.39	0.24	0.08	0.93	0.84	0.30	0.10	1.49	0.97	1.01	10.39	8.18	5.61	9.09	1.76
Na_2O	5.25	4.83	3.72	6.58	5.62	6.72	5.89	4.76	5.15	5.01	5.51	4.18	7.30	7.06	6.43	3.48	4.32	5.08	4.03	3.21
K_2O	5.59	5.45	5.43	5.45	5.64	5.64	4.90	4.58	5.14	6.61	4.85	3.94	5.84	5.67	5.24	1.19	1.74	2.15	1.91	6.10
P_2O_5	0.16	0.14	0.10	0.08	0.42	0.09	0.04	0.06	0.04	0.15	0.05	0.03	0.17	0.09	0.24	0.49	0.73	1.01	0.80	0.33
Sum	100.00	100.00	100.00	100.00	100.00	100.00	100.00	100.00	100.00	100.00	100.00	100.00	100.00	100.00	100.00	100.00	100.00	100.00	100.00	100.00
FeO	3.66	4.36	4.34	4.73	4.67	3.02	3.26	4.94	3.86	2.52	5.10	6.03	1.44	1.42	2.23	8.66	8.93	7.25	8.99	1.89
Fe_2O_3	3.86	3.48	2.19	1.84	1.60	1.98	2.96	0.66	2.79	4.30	2.98	1.09	1.58	1.77	2.37	2.91	2.51	3.89	1.09	2.11
L.O.I.	1.82	1.87	1.47	2.06	0.18	0.66	1.07	1.70	2.55	2.26	3.00	2.54	2.27	1.59	1.62	1.43	1.19	1.83	1.57	3.58
Ba	1331	1823	1091	19	1225	67	50	37	25	936	46	145	863	194	346	387	547	585	1177	1628
Rb	72	89	136	166	51	130	148	190	111	64	209	83	160	160	124	32	33	39	40	225
Sr	77	119	102	28	276	11	9	6	6	40	5	9	539	36	75	610	806	839	1063	293
Zr	685	896	1208	1539	352	1381	1573	2220	908	335	1621	902	1725	1203	816	243	279	403	273	623
Y	56	68	97	119	50	112	80	199	86	32	159	140	103	55	40	33	40	47	34	31
Nb	103	97	85	294	90	245	254	396	150	70	279	195	192	216	155	59	76	92	102	29
F	1080	1343	1264	834	311	1168	2727	287	915		1377		560	155	313	493	772	936	584	
Cl	139	179	127	2464	58	180	132	76	1046		34		219	617	130	177	549	66	635	
La	86.24	104.3	131(A)	268(A)	91.45	187.0	157.9	219.3	110.3	41.16	232.7	430(A)	144.4	147.3	114.9	37.35	47.66	60.86	69.69	290(A)
Ce	177.4	213.6	257(A)	440(A)	173.5	337.1	324.5	422.0	226.9	84.75	406.4	475(A)	241.4	265.4	211.6	76.25	97.65	127.8	125.6	453(A)
Nd	80.20	97.26	128(A)	183(A)	88.57	138.5	130.1	187.0	99.08	41.68	177.6	365(A)	77.07	94.39	70.57	37.95	48.06	65.34	51.01	175(A)
Sm	15.68	18.67			15.52	24.32	24.26	38.24	19.31	8.42	32.03		10.86	14.28	10.69	8.16	10.20	12.81	9.26	
Eu	4.77	5.30			5.36	3.29	2.90	7.84	1.61	4.64	2.98		2.94	2.75	2.18	2.52	3.21	4.04	2.89	
Gd	1.70	14.09			11.64	18.53	17.90	32.14	14.98	7.02	26.61		942.00	11.10	8.17	6.70	7.94	10.61	7.78	
Dy	9.09	11.10			8.53	15.56	14.80	32.97	12.22	5.08	23.36		7.13	8.69	6.67	5.44	6.59	7.48	5.40	
Er	4.33	5.39			3.77	8.18	7.57	18.10	6.05	2.32	12.06		3.96	4.82	3.52	2.47	2.87	3.22	2.49	
Yb	3.92	5.17			3.22	7.27	7.71	17.93	5.85	2.18	12.24		3.93	4.71	3.42	2.05	2.51	2.70	2.00	
Lu	0.65	0.83			0.43	1.16	1.20	2.58	0.90	0.33	1.74		0.61	0.76	0.55	0.30	0.36	0.45	0.32	
Eu/Eu*	1.03	0.96			1.17	0.46	0.41	0.67	0.28	1.11	0.31		0.87	0.64	0.69	1.01	1.05	1.03	1.01	
$(La/Yb)_{en}$	14.79	13.60			19.16	16.88	13.79	8.25	24.79	12.75	12.83		24.79	21.11	22.56	12.28	12.80	15.20	23.49	
$(La/Sm)_{en}$	3.46	3.51			3.69	4.85	4.10	3.61	8.37	3.08	4.57		8.37	6.49	6.75	2.88	2.94	2.99	4.73	
$(Sm/Yb)_{en}$	4.28	3.87			5.19	3.48	3.36	2.28	2.96	4.14	2.81		2.96	3.25	3.34	4.27	4.27	5.08	4.96	
A.I	0.92	0.89	0.82	1.05	0.89	1.10	1.18	0.97	1.00	0.95	1.11	0.96	0.97	1.00	0.94	0.46	0.49	0.51	0.53	0.46
Q	3.71	6.52	16.82	0.00	6.48	4.47	17.03	19.83	12.53	4.00	13.45	21.24	0.00	0.00	1.10	0.00	0.00	0.00	0.00	19.87
Ne	0.00	0.00	0.00	0.00	0.00	0.00	0.00	0.00	0.00	0.00	0.00	0.00	7.05	1.35	0.00	4.62	2.91	0.00	4.95	0.00
Ac	0.00	0.00	0.00	2.74	0.00	2.14	2.66	0.00	0.00	0.00	2.13	0.00	0.00	0.05	0.00	0.00	0.00	0.00	0.00	0.00

Table 3 Representative clinopyroxene, olivine, feldspar and magnetite compositions of the studied silicic volcanics. For clinopyroxenes: Fe_2O_3 calculated after Papike et al. (1974); Fe* = Fe^{2+} + Mn + Fe^{3+}. Abbreviations as in Table 2, except: *Pc* phenocryst, *Gm* groundmass crystal, *Fa* fayalite, *Fo* forsterite, *Tph* tephroite, *Lar* larnite, *Or* orthoclase, *Ab* albite, *An* anorthite

Clinopyroxenes							Olivines		
Sample	CA21	CA21	CA55	CA55	CA152	CA152		CA21	CA21
Type	Pc	Gm	Pc	Gm	Pc	Gm		Pc	Pc
Rock-type	Q-Tr.	Q-Tr.	Q-Tr.	Q-Tr.	Ne-Tr.	Ne-Tr.		Q-Tr.	Q-Tr.
SiO_2	48.64	47.93	51.33	51.60	44.95	49.50		30.06	30.05
TiO_2	0.69	0.48	0.99	0.70	2.58	1.35		0.06	0.03
Al_2O_3	1.48	0.71	1.85	1.00	7.93	1.73		0.00	0.00
FeO_t	23.74	27.20	11.23	12.25	11.75	17.46		63.72	63.66
MnO	0.88	1.04	0.72	1.02	0.48	2.52		2.52	2.61
MgO	4.58	2.22	12.87	11.70	9.04	5.69		3.07	3.29
CaO	20.02	19.41	20.46	20.10	21.92	18.82		1.02	1.08
Na_2O	0.52	0.41	0.53	0.56	1.35	2.90		0.00	0.00
Cr_2O_3	0.06	0.06	0.00	0.00	0.00	0.00		0.00	0.00
Sum	100.61	99.46	99.98	99.56	100.00	99.97		100.45	100.72
Fe_2O_3	1.96	1.15	0.00	0.63	7.10	7.54			
							Fa	87.23	86.55
Ca	43.90	43.56	42.90	42.30	49.78	44.44	Fo	7.49	7.97
Mg	13.75	6.95	37.60	34.20	28.54	48.69	Tph	3.49	3.59
Fe*	42.35	49.49	19.50	23.50	21.69	36.87	Lar	1.79	1.88

Feldpsars							Magnetites			
Sample	CA21	CA21	CA15	CA15	CA152	CA152		CA21	CA65	CA152
Type	Pc	Gm	Pc	Gm	Pc	Pc		Gm	Gm	Gm
Rock-type	Q-Tr.	Q-Tr.	Q-Tr.	Q-Tr.	Ne-Tr.	Ne-Tr.		Q-Tr.	Q-Tr.	Ne-Tr.
SiO_2	60.98	65.64	66.95	66.81	66.22	64.48		0.19	0.26	0.06
TiO_2	0.09	0.02	0.07	0.06	0.00	0.02		18.63	14.57	10.64
Al_2O_3	23.95	19.38	19.14	19.07	19.56	21.72		0.77	0.73	0.16
FeO_t	0.31	0.59	0.34	0.51	0.10	0.34		78.17	81.21	79.63
MnO	0.00	0.00	0.00	0.00	0.00	0.00		0.80	0.68	4.73
MgO	0.00	0.00	0.00	0.00	0.00	0.00		0.04	0.05	0.23
CaO	5.52	0.67	0.17	0.14	0.69	2.87		0.03	0.08	0.04
Na_2O	7.13	5.93	7.84	7.65	6.72	8.99		0.00	0.00	0.00
K_2O	2.02	7.77	5.49	5.76	6.71	1.58		0.00	0.00	0.00
Cr_2O_3	0.00	0.00	0.00	0.00	0.00	0.00		0.00	0.02	0.05
Sum	100.00	100.00	100.00	100.00	100.00	100.00		98.63	97.60	95.54
Or(wt%)	11.97	46.21	32.56	34.21	39.69	9.37	FeO	48.45	44.72	35.98
Ab	60.52	50.44	66.60	65.08	56.90	76.34	Fe_2O_3	33.03	40.54	48.49
An	27.51	3.35	0.84	0.71	3.41	14.30	%Ulvsp.	52.73	41.91	30.32

trachytes (Salviulo et al. submitted). Fongo Tongo peripheral Q-trachytes are characterized by fayalitic (Fa = 87%) olivine phenocrysts.

Peralkaline Q-trachytes have chemical and mineralogical comenditic affinities and are poorly porphyritic or aphyric. The dominant phenocryst and groundmass mineral is a weakly zoned alkali-feldspar ($Ab_{70}Or_{30}$-$Ab_{63}Or_{36}$). Groundmass Fe-augite and Fe-hedenbergite and Ti-magnetite (ulvöspinel = 62%) are rare.

Ne-trachytes (Ngaoundere) contain phenocrysts of alkali-feldspar ($Ab_{73}Or_{22}$-$Ab_{56}Or_{39}$), oligoclase ($An_{14}Ab_{76}$; absent in the peralkaline samples), Mg-rich salites and rare small crystals of Ti-magnetite (ulvöspinel = 30%). Notably, clinopyroxenes from Ne-trachytes show a relatively significant acmitic component (Na = 0.10–0.19 a.f.u.), and suggest a cogenetic origin of strongly alkaline basalts and Ne-trachytes (Salviulo et al. submitted).

Major and trace element compositions

All the silicic rocks investigated (mainly trachytes) have SiO_2 higher than 62 wt%, and are essentially associated with alkaline basalts, minor basanites and their differentiates. A marked SiO_2 gap (55 to 62 wt%) exists between the basaltic and silicic volcanics, also reported by Fitton (1987) and Nono et al. (1994).

The silicic rocks are highly variable in composition (Table 2), as shown, for example, by the Mt. Bambouto (MBT) samples (Fig. 5). MBT samples are characterized by decreasing Al_2O_3, Na_2O and K_2O, and increasing Rb, Zr, Nb and REE with increasing SiO_2, while TiO_2 and FeO_t remain nearly constant. Ba is particularly high (> 1000 ppm) in the least evolved metaluminous Q-trachytes and low (< 100 ppm) in the most differentiated silicic rocks, many of which are peralkaline (Fig. 5b). A

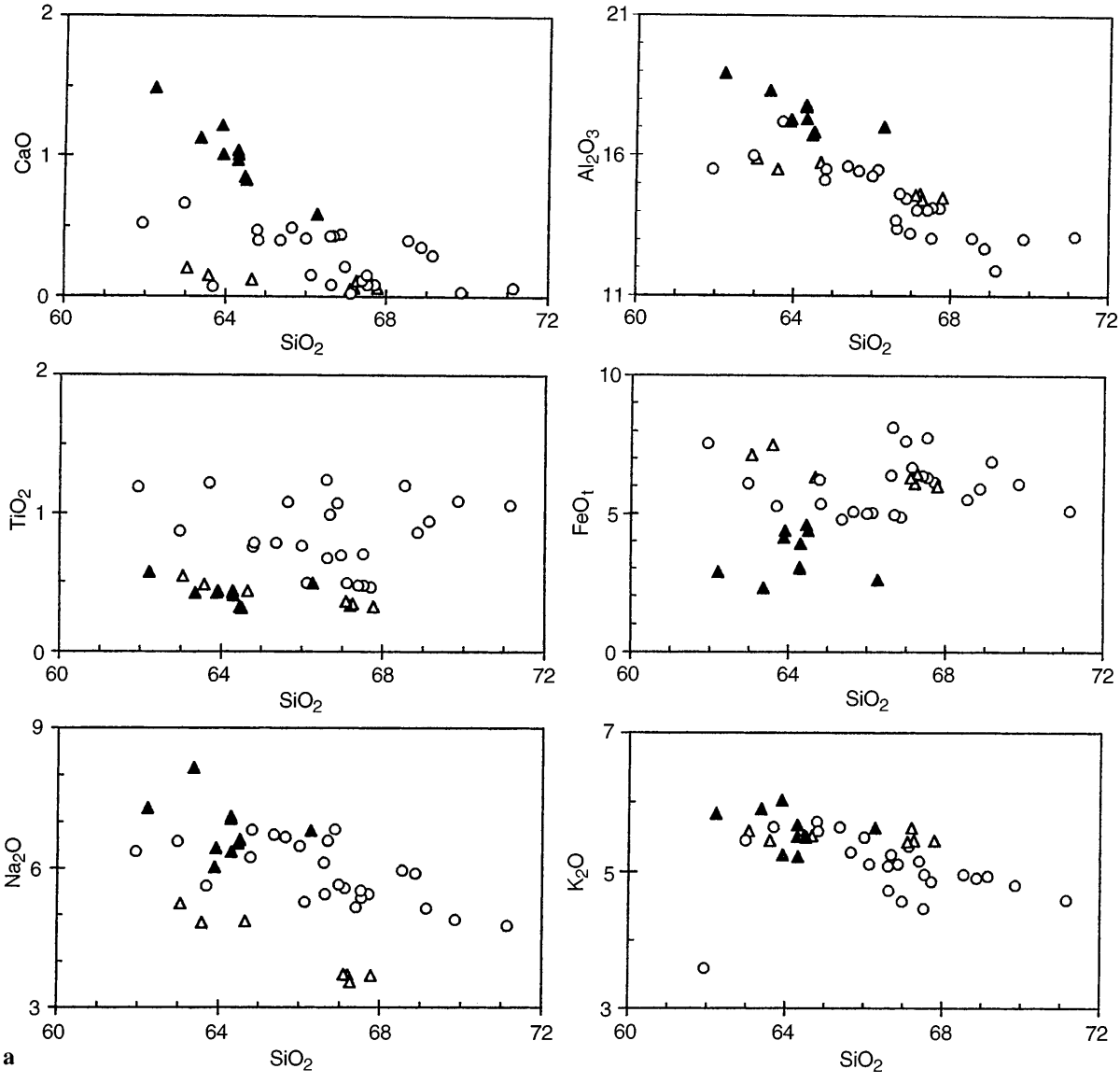

Fig. 5a, b Major (wt%; Fig. 5a) and trace element (ppm; Fig. 5b) variations vs SiO_2 and Zr, respectively, of the studied silicic volcanics. Symbols as in Fig. 2

similar distribution is shown by Sr. Incompatible elements from the MBT silicic rocks (Rb, REE, Zr, Y and Nb; Fig. 5b) show broad positive correlations with the most incompatible elements. Zr and Nb show a well defined linear correlation. It should be noted that the silicic rocks from the top of the Mt. Bambouto volcanic sequence are characterized by higher Zr, Nb and SiO_2 as well as higher $^{87}Sr/^{86}Sr$ initial ratios, relative to those from the lower sections of the silicic sequence (Fig. 6).

The peripheral Q-trachytes from Fongo Tongo and rhyolites from Bandjoun (Mt. Bambouto area) are metaluminous and compositionally different from the other silicic volcanics (Fig. 5), being depleted in Nb (mean 94 vs 248 ppm), enriched in Ba (mean 1452 vs 71 ppm), and with higher K_2O/Na_2O ratios (1.0–1.5 vs 0.5–1.0; cf. Fig. 10). The peripheral Q-trachytes and rhyolites have Zr/Nb ratio increasing from ca. 7 to 16 with differentiation, while other silicic rocks have Zr/Nb of ca. 6 (cf. Figs. 9, 12).

Both the Ngaoundere plateau Ne-trachytes (Ne = 1–7 wt%) and the scarce Q-trachytes (Q = 1–3 wt%) are enriched in Al_2O_3, Na_2O, Ba, Rb and LREE, and depleted in TiO_2, FeO_t and Y, compared with Mt. Bambouto Q-trachytes (Fig. 5).

Chondrite-normalized (cn) REE patterns for Q- and Ne-silicic rocks are shown in Fig. 7 (Table 2). In general, the most evolved samples have a pronounced LREE enrichment, while the MREE/HREE ratio remains nearly constant. Mt. Bambouto, Sabga and Fongo Tongo silicic rocks have $(La/Yb)_{cn}$ and $(Sm/Yb)_{cn}$ ratios ranging from 8.2 to 19.2 and from 2.3 to 5.2, respectively, while the $(Eu/Eu^*)_{cn}$ ratio falls in the

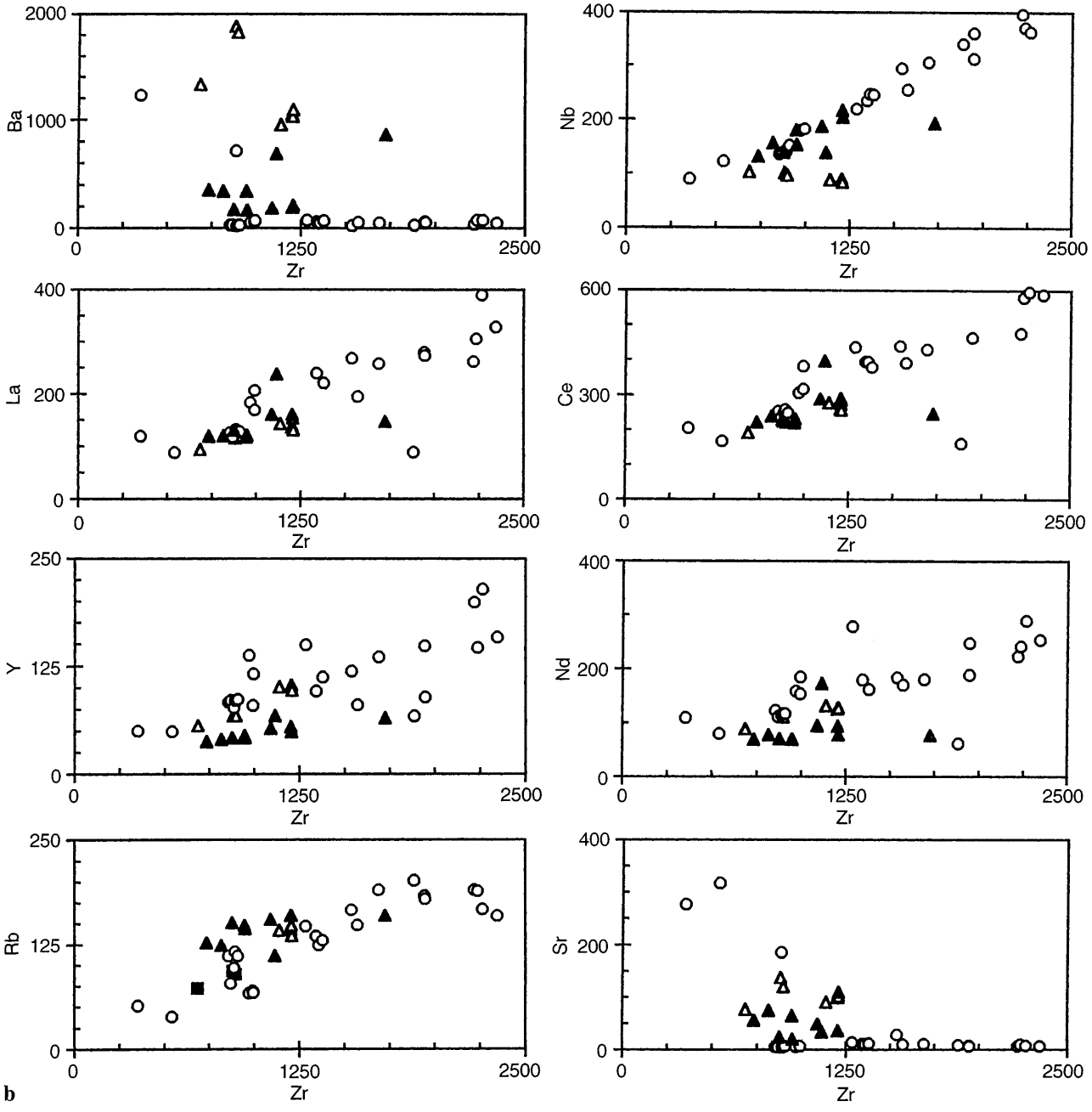

Fig. 5b

0.28–1.17 range. The highest $(Eu/Eu^*)_{cn}$ ratio was obtained from the cumulus feldspar-phyric Mt. Bambouto Q-trachyte (CA10). Ne-trachytes from the Ngaoundere plateau have distinctly higher $(La/Yb)_{cn}$ ratios (21.4–24.8), relative to the other trachytes, while the $(Sm/Yb)_{cn}$ and $(Eu/Eu^*)_{cn}$ ratios, 3.0 vs 3.3 and 0.64 vs 0.87, respectively, are quite similar.

In general, major and trace element relationships revealed that the silicic rocks from the different volcanic centres (e.g. Mt. Bambouto vs Fongo Tongo and Ngaoundere plateau) are compositionally distinct, and that their differentiation appears to be compatible with fractional crystallization, starting from different parental melts (see petrogenetic aspects, below).

Sr, Nd and O isotopic compositions

$^{40}Ar/^{39}Ar$ ages allowed the calculation of reliable initial $^{87}Sr/^{86}Sr$ ratios (Sr_i). The peralkaline Q-trachyte (CA15) and the metaluminous Q-trachyte (CA10) lava flows of the lower portions of the Mt. Bambouto volcanic sequence have Sr_i (0.70361 and 0.70372, respectively; Table 4) similar to those of the associated basic volcanics (0.70311 and 0.70372; Fig. 8; Marzoli 1996). Initial $^{143}Nd/^{144}Nd$ ratios (Nd_i) and $\delta^{18}O$ (whole rock)

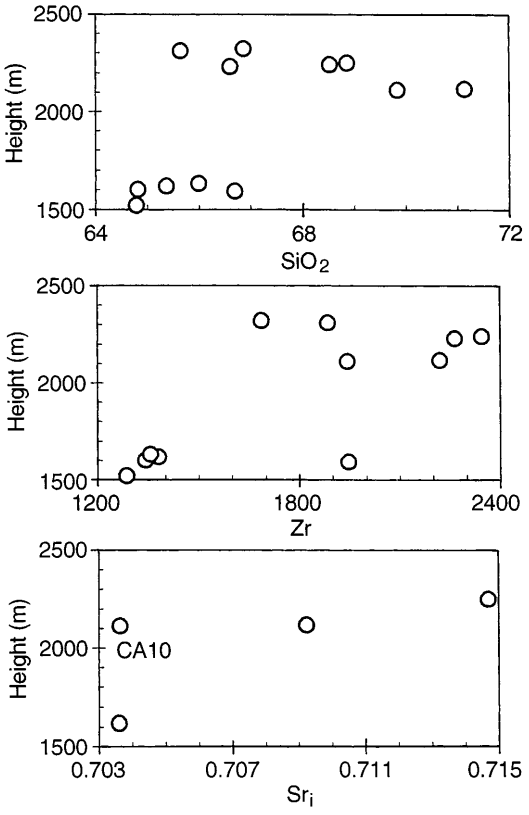

Fig. 6 Variation of SiO_2 (wt%), Zr (ppm) and Sr initial isotopic compositions (Sr_i) vs height (m a.s.l.) of Mt. Bambouto silicic volcanic sequence (cf. Fig. 3). The sample CA10 is alkali-feldspar cumulitic and is shown only for Sr_i

of CA15 and CA10 are 0.512777 and 0.512786, and +6.3‰ and +6.7‰, respectively (Fig. 8; Table 4). Nd_i and $\delta^{18}O$ of these silicic volcanics are in the same range as those of the associated basic volcanics (0.51289–0.51275, and +6.2–+6.8‰, respectively; Marzoli 1996).

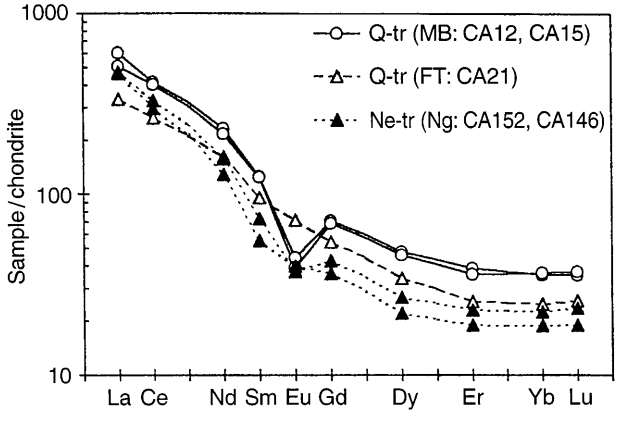

Fig. 7 Chondrite normalized (Boynton 1984) REE concentrations of representative silicic volcanics from Mt. Bambouto (*MB*), Fongo Tongo (*FT*) and Ngaoundere plateau (*Ng*). Symbols as in Fig. 2

The rhyolite CA12 and the peralkaline Q-trachyte CA24 of the upper sections of the Mt. Bambouto volcanic sequence (cf. Fig. 3) are characterized by high Sr_i (0.70946 and 0.71462, respectively) and $\delta^{18}O$ (+9.1‰, CA12, whole rock) and by relatively low Nd_i (0.512635 and 0.512680, respectively; Fig. 8). These silicic rocks (Table 2) are characterized by high SiO_2 (>67 wt%), Zr (>1570 ppm), Nb (>250 ppm), Nd (>130 ppm), and low Sr (8–9 ppm). The isotopic compositions of these silicic rocks, compared with those of the underlying Q-trachytes, suggest that crustal contamination has to be considered in their genesis. As expected, the most important isotopic variations relate to Sr_i, as CA12 and CA24 are characterized by very low Sr (<10 ppm).

The Fongo Tongo Q-trachytes (CA21 and CA23) and the Bandjoun rhyolites (CA65 and CA66) are characterized by moderately high Sr_i (0.70534–0.70586 and 0.70851–0.70861, respectively), $\delta^{18}O = +8.1$‰ (CA23, whole rock), and by low Nd_i (CA21, 0.512458 and CA65, 0.512346), distinct from those for the MBT silicic rocks, and CVL basalts (Fig. 8).

Finally, Ne-trachytes (CA152 and CA146; 9.3 and 11.4 Ma, respectively) from the Ngaoundere plateau have Sr_i ratios (0.70393 and 0.70563, respectively) lower than that (0.70642) of the associated Q-trachyte (CA138).

Petrogenetic aspects

Sr, Nd and O isotopic data indicate that some of the Q- and Ne-trachytes have characteristics similar to those of mantle-derived rocks, as do the associated alkaline basalts. The isotopic data suggest that assimilation of high Sr_i and low Nd_i crustal material (e.g. the Pan-African granitic basement) was absent or negligible. In this case the genesis of the Q-trachytic magmas may be related to fractional crystallization of the associated alkaline basalts or by melting of compositionally appropriate basic crustal materials.

Closed system evolution

Despite the compositional gap between the investigated basic and silicic samples (see silica gap, below), we modeled the transition from alkaline basalts to the least evolved trachytic rocks through fractional crystallization, using major (Stormer and Nicholls 1978; Ghiorso and Sack 1995: MELTS code) and trace (Rayleigh fractionation; Arth 1976) elements.

The whole rock compositions, modeled as parental magmas to Q- and Ne-trachytes (CA15 and CA152, respectively), are the hawaiite CA38 (Ne = 3 wt%), the Hy-mugearite CA172 (Ol/Hy = 1.28), and the hawaiite CA133 (Ne = 5 wt%; Table 2). The selected basaltic rocks are aphyric and have low Sr_i ratios (0.70328–0.70361), as do the selected Q- and Ne-trachytes (0.70361–0.70393).

Table 4 Sr, Nd and O isotopic compositions of continental CVL silicic and representative basic volcanics. Errors are at the 2σ level, except for $\delta^{18}O$ (1σ). The reported ages are those considered for the calculations of initial isotopic ratios (Sr_i, Nd_i). Rb and Sr concentrations were measured by XRF, and Sm and Nd by ICP-MS (Table 2). Parameters used for calculations of ε_{Sr} and ε_{Nd} are from Faure (1987). Abbreviations as in Table 2

Sample	CA23	CA21	CA10	CA15	CA24	CA12	CA40	CA38
Rock-type	Q-Tr.	Q-Tr.	Q-Tr.	Q-Tr.	Q-Tr.	Rhy.	Alk.Bas.	Haw.
Area	F.To.	F.To.	Bamb.	Bamb.	Bamb.	Bamb.	Bamb.	Bamb.
Age	15Ma	15Ma	16Ma	17Ma	16Ma	16Ma	19Ma	19Ma
Rb/Sr	0.94	0.75	0.18	11.82	16.44	31.67	0.05	0.04
$(^{87/86}Sr)_m$	0.70592(2)	0.70632(4)	0.70384(1)	0.71213(2)	0.72613(2)	0.73046(2)	0.70311(2)	0.70325(2)
$(^{87/86}Sr)_i$	0.70534(2)	0.70586(4)	0.70372(1)	0.70361(2)	0.71462(2)	0.70946(2)	0.70310(2)	0.70324(2)
$\varepsilon^T Sr$	12.17	19.55	−10.83	−12.34	143.90	70.65	−19.48	−17.50
Sm/Nd	0.20	0.19	0.18	0.18	0.19	0.20	0.22	0.21
$(^{143/144}Nd)_m$		0.512457(3)	0.512785(4)	0.512776(6)	0.5126879(9)	0.512634(8)	0.512841(3)	0.512853(5)
$(^{143/144}Nd)_i$		0.512458(3)	0.512786(4)	0.512777(6)	0.512680(9)	0.512635(8)	0.512843(3)	0.512854(5)
$\varepsilon^T Nd$		−3.12	3.26	3.09	1.20	0.32	4.38	4.59
$\delta^{12}O$	8.1(4)		6.7(4)	6.3(2)		9.1(5)	6.3(2)	6.4(3)

Sample	CA65	CA66	CA59	CA152	CA146	CA138	CA172	CA133
Rock-type	Rhy.	Rhy.	Q-Tr.	Ne-Tr.	Ne-Tr.	Q-Trac.	Mug.	Haw.
Area	Bandj.	Bandj.	Sabga	Nga.	Nga.	Nga.	Oku	Nga.
Age	15Ma?	15Ma?	22Ma	9Ma	11Ma	10Ma	23Ma	<10Ma
Rb/Sr	1.33	1.42	18.50	0.30	4.44	1.65	0.04	0.04
$(^{87/86}Sr)_m$	0.70932(4)	0.70848(2)	0.72204(2)	0.70405(1)	0.70693(1)	0.70710(1)	0.70361(1)	0.70328(2)
$(^{87/86}Sr)_i$	0.70851(4)	0.70861(2)	0.70528(2)	0.70393(1)	0.70563(1)	0.70642(1)	0.70360(1)	0.70327(2)
$\varepsilon^T Sr$	57.17	58.59	11.32	−7.84	16.29	27.50	−12.39	−17.07
$\delta^{12}O$			9.5(2)					

Hawaiite to Q-trachyte transition

According to mass balance results (Stormer and Nicholls 1978) the transition from the hawaiite CA38 to the Q-trachyte CA9 is compatible ($Res.^2 = 0.81$) with 74 wt% fractional crystallization of plagioclase (45.5 wt%), clinopyroxene (11.6 wt%), magnetite (10.5 wt%), olivine (5.2 wt%) and apatite (1.2 wt%) (Table 5). Mineral compositions used in the modeling are reported in Table 6. The feasibility of this transition is broadly consistent with (Rayleigh fractionation) trace element modeling (Table 5), using the partition coefficients (Table 7) of LeMarchand et al. (1987), Mahood and Stimac (1990), and Green (1994). As expected, the transition from the Hy-mugearite CA172 to the Q-trachyte CA9 is also compatible ($Res.^2 = 0.16$) through 68 wt% fractional crystallization of plagioclase (44.6 wt%), magnetite (9.1 wt%), clinopyroxene (6.7 wt%), olivine (5.2 wt%) and apatite (1.2 wt%). It should be noted that calculations indicate that the transition to the Q-trachyte CA9 is unlikely ($Res.^2 > 1.6$) starting from the more undersaturated hawaiite CA133 (Ne = 5 wt%) as a parental basaltic magma.

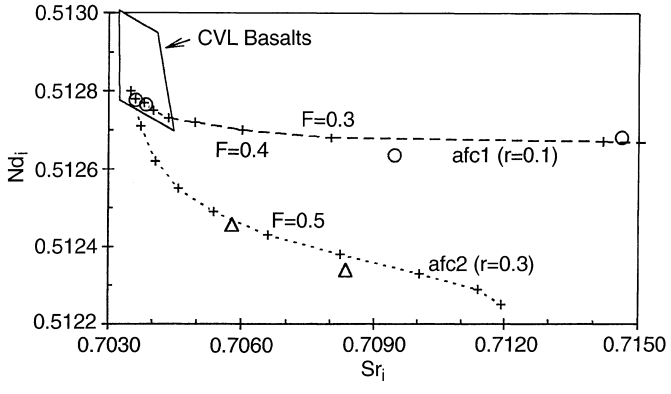

Fig. 8 Sr_i vs Nd_i (and Sr_i vs $\delta^{18}O$, inset) composition of silicic CVL volcanics: Mt. Bambouto (*filled circles*) and Fongo Tongo and Bandjoun (*open triangles*). The open box represents the field of CVL basic volcanics (Halliday et al. 1988; Marzoli 1996). For AFC calculations (DePaolo 1981) the following parameters are assumed: *uncontaminated magma*: Sr = 900 ppm, Nd = 60 ppm, $Sr_i = 0.7035$ and $Nd_i = 0.5128$; *contaminant* "*afc1*": Sr = 300 ppm, Nd = 180 ppm, $Sr_i = 0.7120$ and $Nd_i = 0.5125$; *contaminant* "*afc2*": Sr = 300 ppm, Nd = 60 ppm, $Sr_i = 0.7120$ and $Nd_i = 0.5120$. The calculated bulk solid/liquid partition coefficients for Sr and Nd are 3 and 0.1, respectively. "*r*" rate of assimilated mass/rate of fractionated mass. *F* fraction of residual liquid (*tick marks* represent 10% intervals)

MELTS modeling suggests that the transition from the hawaiite CA38 or the Hy-mugearite CA172 to the Q-trachytes (e.g. CA9) is compatible with fractional crystallization at low pressure (1 kbar), QFM buffer conditions and low (0.5 wt%) H_2O content in the starting basaltic magmas (Figs. 9, 10). Note that the large collapse calderas of Mt. Bambouto and Mt. Oku indicate shallow level magma chambers, probably only a few kilometers deep (cf. Mahood 1984). QFM and near anhydrous conditions are consistent with the slightly alkaline nature of the assumed parental basalt (cf. Mahood and Baker 1986; Carmichael 1991; Brotzu et al. 1997; Dixon et al. 1997), and with the observed mineral assemblages of the alkaline basalts

Table 5 Mass balance and Rayleigh results for fractional crystallization from parental to derived magmas (cf. Table 2 for compositions). The amount of fractionated minerals (compositions in Table 6), the sum of the squares of major element residuals (Res.^{2}) and the calculated vs observed trace element concentrations (calc./obs.) are shown. Mass balance results of melting modeling (CA40 to CA9) are also reported. (*ol* olivine, *cpx* clinopyroxene, *plg* plagioclase, *akf* alkali-feldspar, *mt* magnetite, *ap* apatite)

Crystal Fractionation						Melting
Parental	CA38	CA172	CA133	CA9	CA15	CA40
Derived	CA9	CA9	CA152	CA15	CA24	CA9
Fractionating Minerals (wt%)						
ol	5.17 (Fa_{71})	5.19 (Fa_{71})	12.84 (Fa_{71})	–	–	6.58 (Fa_{86})
cpx	11.59 (Salite)	6.66 (Salite)	13.87 (Salite)	3.31 (Fe-Aug.)	1.31 (Fe-Aug.)	30.23 (Salite)
plg	45.48 (An_{35})	44.55 (An_{35})	34.01 (An_{62})	0.11 (An_{35})		25.7 (An_{68})
akf	–	–	–	38.23	56.17	–
mt	10.45	9.11	6.45	3.40	2.70	8.28
ap	1.25	1.24	1.84	0.07	–	1.16
Sum	73.93	66.75	61.63	45.12	60.16	71.96
Res.^{2}	0.818	0.158	0.605	0.209	0.300	0.461
calc./obs.						
Ba	2.60	2.68	1.09	0.05	0.02	21.65
Rb	0.93	0.84	0.77	1.98	1.99	0.52
Sr	1.07	1.15	0.76	0.38	0.04	29.54
La	0.87	0.79	1.32	2.26	2.66	0.34
Ce	0.98	1.01	1.34	1.81	2.38	0.45
Nd	1.10	0.97	1.08	2.13	2.40	0.43
Zr	0.80	0.93	0.65	1.54	1.76	0.38
Nb	0.87	0.96	1.52	1.64	3.34	0.59
Y	1.14	1.20	0.89	1.88	2.18	0.48

Table 6 Mineral compositions of CVL basic and silicic volcanics (Marzoli 1996) used in mass balance calculations (cf. Table 5). Apatite composition after Deer et al. (1978). Abbreviations as in Table 6

Mineral	ol	ol	cpx	cpx	plg	plg	plg	akf	mt	apatite
Sample	CA54	CA75	CA75	CA60	CA54	CA25	CA50	CA60	CA33	
Name	Fo_{64}	Fo_{71}	Salite	Fe-Augite	An_{40}	An_{42}	An_{28}	Sanidine		
SiO_2	40.38	37.90	49.31	49.44	50.47	52.06	59.62	66.66	0.14	0.00
TiO_2	0.00	0.00	1.70	0.44	0.14	0.27	0.08	0.04	19.76	0.00
Al_2O_3	0.06	0.01	4.73	0.60	31.20	29.98	25.19	19.21	0.77	0.00
FeO_t	12.54	24.69	8.61	21.08	0.61	0.64	0.17	0.28	79.06	0.22
MnO	0.09	0.52	0.30	1.49	0.00	0.00	0.00	0.00	0.20	1.59
MgO	46.70	36.54	14.14	5.63	0.00	0.00	0.00	0.00	0.04	0.56
CaO	0.23	0.34	20.43	20.79	13.96	12.59	6.87	0.29	0.03	54.78
Na_2O	0.00	0.00	0.78	0.53	3.40	4.03	7.08	7.21	0.00	0.00
K_2O	0.00	0.00	0.00	0.00	0.22	0.43	0.99	6.31	0.00	0.00
P_2O_5	0.00	0.00	0.00	0.00	0.00	0.00	0.00	0.00	0.00	42.85
Sum	100.00	100.00	100.00	100.00	100.00	100.00	100.00	100.00	100.00	100.00

Table 7 Mineral/melt partition coefficients used in Rayleigh fractionation modeling. Data are from LeMarchand et al. (1987), Mahood and Stimac (1990) and from Green (1994). "*h*" and "*t*" are the partition coefficients used for hawaiite-trachyte and inter Q-trachytes fractionation, respectively. Abbreviations as in Table 5

	ol	cpx-h	cpx-t	plg-h	plg-t	akf	mt	ap
Ba	0.01	0.01	0.10	3.00	5.00	6.00	0.01	0.01
Rb	0.01	0.01	0.01	0.05	0.11	0.11	0.07	0.01
Sr	0.01	0.10	0.10	4.00	5.00	5.00	0.15	5.00
La	0.01	0.05	0.28	0.01	0.10	0.04	0.08	5.00
Ce	0.01	0.30	0.48	0.01	0.04	0.04	0.08	5.00
Nd	0.01	0.60	0.80	0.01	0.01	0.04	0.08	6.00
Zr	0.01	0.05	0.50	0.02	0.15	0.10	0.35	0.01
Y	0.01	0.50	1.50	0.01	0.01	0.01	0.04	5.00
Nb	0.01	0.01	0.01	0.01	0.01	0.01	1.00	0.01

and associated Q-trachytes (cf. Lowsteren and Mahood 1991; Thy and Lofgren 1992; Wilding et al. 1993). Finally, we note that MELTS fractionating minerals and their amounts are similar to those obtained by mass balance calculations (Fig. 10b).

Hawaiite basalt to Ne-trachyte transition

Mass balance results (Table 5) indicate that Ne-trachyte CA152 (Ngaoundere plateau) can be derived (Res.^{2} = 0.61) from the hawaiite CA133 by 62 wt% fractional crystallization of plagioclase (34.0 wt%), clinopyroxene (13.9 wt%), olivine (12.8 wt%), magnetite (6.5 wt%) and apatite (1.8 wt%). This transition is

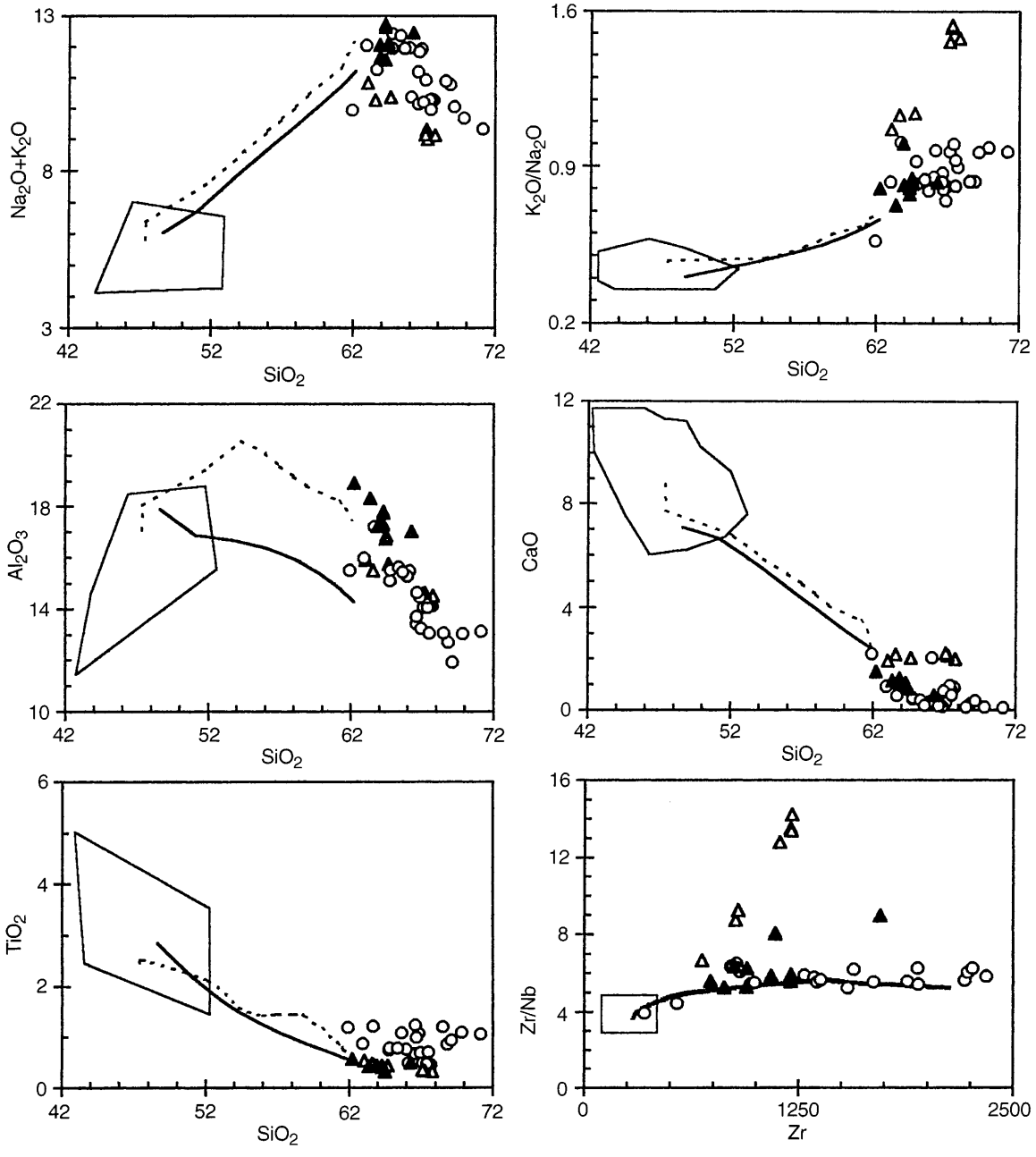

Fig. 9 Closed system fractional crystallization liquid lines of descent calculated using MELTS (Ghiorso and Sack, 1995). *Solid and dashed lines* differentiation paths of CA38 and CA133, respectively (see text and Figs. 10, 11 for details). Zr vs Zr/Nb variation was calculated (Rayleigh fractionation) using the wt% of fractionated minerals and of residual liquid obtained with MELTS, and the partition coefficients of Table 7. Symbols for silicic volcanics as in Fig. 5. *Open boxes* compositional field of continental CVL basic volcanics (Marzoli 1996)

broadly supported by the calculated trace element contents (Table 5). The adopted mineral compositions and trace element partition coefficients are in Tables 6 and 7, respectively.

MELTS modeling indicates (Figs. 9,11) that the fractional crystallization transition from the hawaiite CA133 to Ne-trachyte CA152 requires f_{O_2} values corresponding to QFM + 2 log units, $H_2O = 1.0$ wt%, and variable pressure (6 to 2 kbar). The fractionation at 6 kbar is necessary to suppress early plagioclase saturation in order to account for the high Al_2O_3 (and Ba and Sr) content of Ne-trachytes. Note that (Fig. 11) MELTS modeling includes orthopyroxene as a liquidus phase (ca. 5 wt%), while mass balance calculations and petrography suggest olivine fractionation. In MELTS modeling the magma is assumed to rise to shallower depths, after about 40 wt% fractionation. The second fractionation step at lower pressure (2 kbar; still at QFM + 2) is dominated by plagioclase and magnetite. We note that the polybaric fractional crystallization process guarantees the best match between modeled and

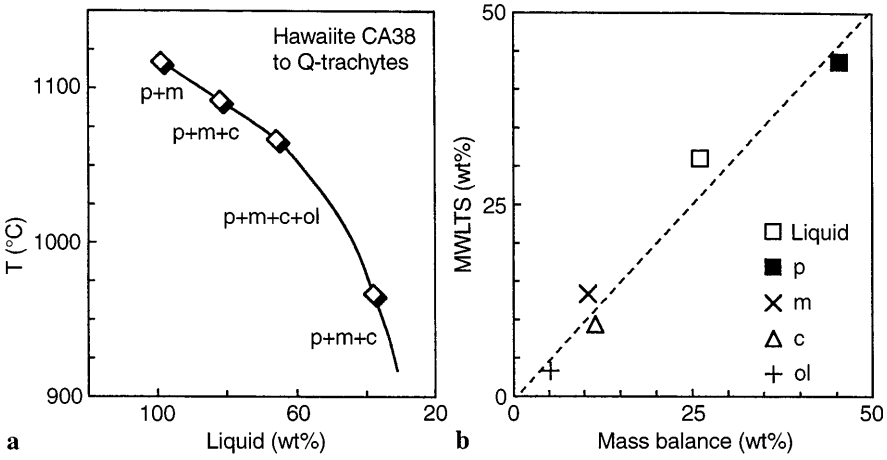

Fig. 10a, b Fractional crystallization modeling from hawaiite CA38 to Q-trachytes at 1 kbar, QFM buffer and 0.5 wt% H_2O in the starting magma. Fig. 10a: fractionating mineral assemblages vs liquidus temperature (T °C). Fig. 10b: MELTS results vs mass balance results (CA38 to CA9; cf. Table 5). *Liquid* residual melt, *p* plagioclase, *c* clinopyroxene, *m* magnetite, *ol* olivine

observed mineral assemblages and compositions, and liquid lines of descent of Ngaoundere magmatic rocks. Notably, 6 kbar corresponds approximately to P_t at the base of the crust under the Ngaoundere Plateau (ca. 20 km depth).

Silica gap

An important problem concerning the petrogenesis of the Cameroon trachytes is to explain the SiO_2-gap (55–62 wt%) between the closely associated basic and silicic volcanics. MELTS fractional crystallization models indicate that the silica gap corresponds to a relatively small liquid fraction, ca. 10–15 wt%. It follows that the extrusion of the latter melts is strongly dependent on the tectonic regime. If extensional tectonics is quite active during magma differentiation, the volumes of the outpoured melts approach those expected in terms of fractional crystallization (e.g. Boina central volcanoes: Afar Depression, East Africa; Barberi et al. 1974). By contrast, if extensional strain is relatively low (e.g. Fantale central volcano, Main Ethiopian Rift, East Africa; Gibson 1974), most of the volcanism is silicic since the most evolved magmas of zoned magmatic chambers are preferentially extruded. Notably, central volcanoes from the Main Ethiopian Rift are characterized by large collapse calderas.

Similarly, the dominantly silicic nature of the Mt. Bambouto and Mt. Oku central volcanoes and the virtual absence of volcanics with intermediate compositions may be due to a relatively low extensional tectonic permissivity in the continental sector of the CVL, and to the relatively small fraction of residual melts corresponding to 55–62 wt% silica gap. This is consistent with the rapid extrusion of the voluminous silicic volcanics (< 2.7 Ma, compared to a lifespan of ca. 20 million years of the associated basic volcanism at Mt. Bambouto, for example) from shallow level magma chambers, and the subsequent formation of collapse calderas.

Another possible explanation of the SiO_2 gap implies that CVL silicic magmas may have formed from lower crust by melting of compositionally appropriate materials (e.g. mafic granulites, amphibolites), or underplated CVL basalts similar to those associated with the silicic

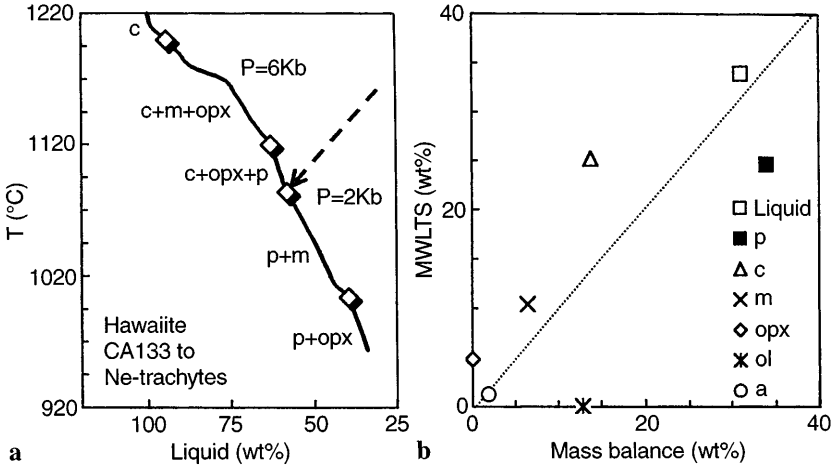

Fig. 11a, b Fractional crystallization modeling, as in Fig. 10, considering the hawaiite CA133 as starting magma, QFM + 2, 1 wt% H_2O, and two pressure evolutionary stages at 6 and 2 kbar (the transition is shown by the *arrow*), respectively. Mass balance calculations relate to the fractional crystallization transition from CA133 to Ne-trachyte CA152 (Fig. 11b). *opx* orthopyroxene, *a* apatite, other abbreviations as in Fig 10

volcanics. Mass balance results (Res.^{2} > 2) indicate that granulites and amphibolites are not suitable materials to generate the investigated Q- and Ne-trachytes (cf. Beard and Lofgren 1991). On the other hand, moderately alkaline basalts (e.g. CA40, Ne = 7 wt%) may represent appropriate source materials for major but not for trace elements (batch melting; Hanson 1978): Sr and Ba contents would be (Table 5) about 20 times higher than those observed (cf. Mungall and Martin 1995; Hay and Wendlandt 1995).

Q-trachytic magma differentiation

The differentiation of the least evolved Q-trachytes to rhyolites is compatible with fractional crystallization according to major element mass balance calculations (Table 5). For example, the transition from CA9 (SiO_2 = 63 wt%) to CA15 (SiO_2 = 65 wt%) is compatible (Res.^{2} = 0.21) with ca. 46 wt% removal of alkali feldspar (38.3 wt%), Fe-augite (3.3 wt%), magnetite (3.4 wt%), plagioclase (0.1 wt%) and apatite (0.1 wt%). The transition from CA15 to the peralkaline Q-trachyte CA24 (SiO_2 = 69 wt%; A.I. = 1.18) is compatible (Res.^{2} = 0.30) with 60 wt% fractionation of alkali feldspar (56.2 wt%), magnetite (2.7 wt%) and Fe-augite (1.3 wt%). Similarly, MELTS modeling points to the feasibility of fractional crystallization in the trachytic-rhyolitic magma differentiation at 1 kbar, QFM buffer and H_2O = 1–1.5 wt%, through alkali feldspar fractionation (ca. 90 wt%).

Trace element modeling (Rayleigh fractionation) results show that there is a marked difference between calculated and observed contents (Table 5). This cannot be easily related to an erroneous choice of the partition coefficients, but suggests differentiation processes other than simple fractional crystallization (cf. Macdonald 1987).

Open system evolution

Many investigated silicic rocks yield higher Sr_i and $\delta^{18}O$, and lower Nd_i than those of the associated basalts (Fig. 8) suggesting interaction with crustal materials. The few known isotopic compositions of crustal samples belonging to the CVL Pan-African basement are those of the xenoliths found in alkaline basalts from Mt. Bambouto (Fitton, written communication, 1994). The isotopic compositions of these crustal xenoliths ($^{87}Sr/^{86}Sr$ = 0.71043–0.72099, $^{143}Nd/^{144}Nd$ = 0.51215–0.51165 and $\delta^{18}O$ = +9‰ and +13‰, respectively; Halliday et al. 1988) are used hereafter as contaminants in AFC calculations (afc1 and afc2, respectively, in Figs. 8 and 12). The composition of a basement Pan-African granite (near Mt. Bambouto; Table 2, CA18) was used for contamination modeling in terms of major and trace elements.

Mt. Bambouto

High Sr_i isotopic ratios (0.70946–0.71462) characterize the most evolved silicic samples (CA12, CA24) from the upper stratigraphic sections of the Mt. Bambouto volcanic sequence. As previously shown, these silicic volcanics may have been formed through ca. 70–80 wt% of feldspar-dominated fractionation (Table 5) from Sr-rich (> 600 ppm) alkaline basaltic melts characterized by low Sr_i ratios (e.g. < 0.70372). The calculated bulk distribution coefficient for Sr is about 3, and then a low value of r (rate of assimilated mass/rate of fractionated mass) is required to achieve relatively high Sr isotopic composition. AFC modeling (DePaolo 1981) requires an r value of 0.1 to match Sr and Nd isotopic compositions (i.e. 0.7095–0.7146 and 0.512635–0.512680, respectively) of the crustally contaminated silicic volcanics of Mt. Bambouto (afc1 path in Fig. 8). Owing to the low Sr (< 10 ppm) of these evolved silicic samples, the high Sr_i ratios are compatible with small contamination by Pan-African granites (e.g. Sr_i = 0.7210: Halliday et al. 1988). By contrast, the high Nd elemental content (150–250 ppm), makes Nd isotopic ratio less sensitive, relative to Sr_i, to crustal contamination. According to Cavazzini (1996), ca. 45 wt% of Sr and ca. 20 wt% of Nd of the above contaminated silicic volcanics would be derived from the contaminant (Fig. 13, inset). As expected, the moderate assimilation of granitic material cannot change appreciably the bulk compositions of the contaminated rocks.

Fongo Tongo and Bandjoun

These silicic rocks have high Sr_i (0.70581–0.70861) and whole rock $\delta^{18}O$ (+8.1, CA23) values, and low Nd_i compositions (0.512458–0.512346). These isotopic data and the high K_2O/Na_2O, La/Nb and Zr/Nb ratios in-

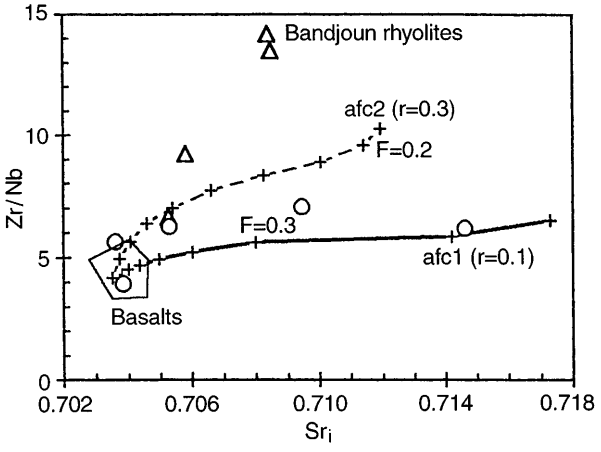

Fig. 12 Sr_i vs Zr/Nb of Mt. Bambouto (*filled circles*) and Fongo Tongo and Bandjoun (*open triangles*) silicic volcanics. "*afc1*" and "*afc2*", as in Fig. 8. Zr and Nb concentrations of the contaminant are those of the basement granite CA18 (Table 2)

dicate that an AFC contamination process would involve a larger contamination degree and/or a quite different crustal contaminant (afc2 path in Figs. 8 and 12).

AFC ("r" = 0.3) and MELTS results indicate that major and trace elements of the Fongo Tongo Q-trachyte CA21, can result from ca. 50 wt% fractionation and ca. 20 wt% of granite assimilation starting from an uncontaminated basaltic magma, i.e. hawaiite CA38. Bandjoun rhyolites seem to require, instead, higher amount of contamination and/or compositionally different crustal contaminants (Fig. 8).

Ngaoundere plateau trachytes

The silicic volcanics of the Ngaoundere plateau are characterized by Sr_i isotopic ratios which increase from Ne (0.70393–0.70563) to Q-trachytes (0.70642). It should be noted that the lowest Sr_i ratio (0.70393, CA152) is higher than those of the associated Ngaoundere basic volcanics (i.e. 0.70289–0.70348; Marzoli 1996). The sample CA152 has higher Sr relative to the other (CA146 and CA138) Ne- and Q-trachytes (i.e. 539 vs 40 and 80 ppm, respectively), and is therefore less sensitive to crustal contamination in terms of Sr isotopes. AFC calculations revealed that Sr isotopic compositions of both Ne and Q-trachytes of the Ngaoundere plateau may be obtained using an r value of 0.1, starting from an alkaline basic magma ($Sr_i = 0.7034$; Sr = 600 ppm). Different relative amounts of feldspar fractionation in the petrogenesis of Ne and Q-trachytes (Fig. 13) guarantee different AFC evolution paths in terms of Sr isotopic compositions (inset of Fig. 13).

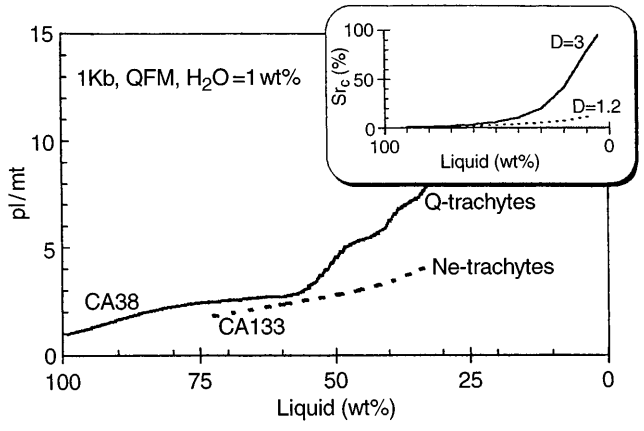

Fig. 13 Residual liquid (wt%) vs feldspar/magnetite (*pl*/*mt*) fractionation as calculated by MELTS, assuming CA38 (*solid line*) and CA133 (*dashed line*) as starting magma compositions. Same conditions as in Fig. 10. Different amounts of feldspar fractionation allow for different bulk partition coefficients for Sr (D_{Sr} calculated to be 3 and 1.2 in the differentiation from CA38 to Q-trachytes and from CA133 to Ne-trachytes, respectively). Therefore, (*inset*) the wt% of Sr derived from the contaminant (Sr% (cont.)) is higher in Q-trachytes (*solid and dashed lines*, respectively)

Conclusions

(1) The silicic volcanism of Mt. Oku, Sabga area and Mt. Bambouto (Western Cameroon Highlands, WCH) occurred between 25 and 15 Ma and is represented by voluminous Q-trachytes and minor rhyolitic ignimbrites. At Mt. Bambouto central volcano about 700 m of precalderic silicic volcanics were erupted in less than 2.7 Ma. These silicic volcanics are associated with slightly to moderately alkaline basalts and minor basanites. In general, the onset of the silicic volcanism migrated from NE (Oku: 25 Ma) to SW (Sabga: 23 Ma, Bambouto: 18 Ma, and near Manengouba: 12 Ma; Dunlop, 1983).

(2) The silicic volcanism on the Ngaoundere plateau (Eastern Cameroon Highlands, ECH) is younger (11-9 Ma) than that of WCH and is compositionally distinct, being composed of Ne-trachytes and rare Q-normative types. This SiO_2-undersaturated silicic volcanism is mainly associated with basanitic rocks.

(3) The lower portions of the silicic volcanism of WCH (Oku, Sabga area and Bambouto) are less evolved than the upper ones which also have high values of Sr_i and $\delta^{18}O$ and low Nd_i. The least differentiated silicic volcanics are isotopically similar to the associated alkaline basalts suggesting differentiation processes without appreciable interaction with crustal materials, which, instead, may have played some role in the genesis of the most evolved silicic volcanics.

(4) Q-trachytes and rhyolites erupted from peripheral vents (Fongo Tongo and Bandjoun) have Sr-Nd-O isotopic compositions markedly different from those of mantle derived CVL basalts, suggesting that these silicic magmas were significantly contaminated by Pan-African granites.

The SiO_2-undersaturated silicic volcanics of Ngaoundere have variable Sr isotope compositions which indicate variable and moderate crustal contamination.

(5) Fractional crystallization is the preferred model for the genesis of the silicic melts of both WCH and ECH. This process sometimes occurred concurrently with crustal contamination. The parental magmas would be the associated alkaline basic products: slightly to moderately alkaline basalts for the Q-silicic volcanics of WCH, and more alkaline melts for the Ne-silicic rocks of ECH.

(6) The virtual absence of volcanics compositionally intermediate between the basic and silicic products (silica gap between 55–62 wt%) could be related to the relatively minor role of extension of the crust in the continental sector of CVL, as well as to the small (10–15 wt%) liquid fraction of the magmas with intermediate compositions.

(7) The migration (25 to 12 Ma) of the silicic volcanism in the continental sector of CVL is reminiscent of that (31–5 Ma) of the onset of the basic volcanism in the oceanic sector (Lee et al. 1994a) of CVL. These ages, and that (11–9) of the silicic volcanism of the Ngaoundere

plateau, indicate that the Cameroon Volcanic Line as a whole may not be easily interpreted as the surface expression of hot spot magmatism. The migration of the volcanism occurring at the same time along the aligned WCH and oceanic volcanoes suggests distinct thermal anomalies, during the SW-NE migration of the African plate (Pollitz 1991; Silver et al. 1998).

Acknowledgements We are grateful to A. Cundari for the critical review and helpful suggestions of an earlier version of the manuscript. We thank L. Furlan and R. Zettin (Trieste), A. Giaretta and R. Carampin (Padova) and T. Becker (Berkeley) for their technical and analytical collaboration. Support from Italian (CNR and MURST) and Brazilian (PADCT/FINEP) agencies is gratefully acknowledged. A.M wishes to thank BGC staff for their friendly hospitality and constant help during his visits in Berkeley. Geochronology studies at BGC were supported by the Ann and Gordon Getty Foundation. Careful reviews by G. Fitton and by D.R. Baker helped to improve the manuscript substantially.

References

Arth JG (1976) Behavior of trace elements during magmatic processes – summary of theoretical models and their applications. J Res US Geol Surv 4: 41–47

Barberi F, Ferrara G, Santacroce R, Treuil M, Varet, J (1974) A transitional basalt-pantellerite sequence of fractional crystallization; the Boina center (Afar rift, Ethiopia). J Petrol 16: 25–56

Beard JS, Lofgren GE (1991) Dehydration melting and water saturated melting of basaltic and andesitic greenstones and amphibolites. J Petrol 32: 365–401

Boynton WV (1984) Cosmochemistry of rare earth elements: meteorite studies. In: Henderson P (ed) Rare earth element geochemistry. Elsevier, Amsterdam, pp 63–114

Brotzu P, Gomes CB, Melluso L, Morbidelli L, Morra V, Ruberti E (1997) The alkaline igneous complex of Itatiaia, SE Brazil: role of fractional crystallization and crustal contamination in the petrogenesis of coexisting Si-undersaturated to Si-oversaturated felsic rocks. Lithos 40: 133–156

Carmichael ISE (1991) The redox state of basic and silicic magmas: a reflection of their source? Contrib Mineral Petrol 106: 36–64

Cavazzini G (1996) Degrees of contamination in magmas evolving by assimilation-fractional crystallization. Geochim Cosmochim Acta 60: 2049–2052

Deer WA, Howie RA, Zusmann J (1978) An introduction to the rock-forming minerals. Longmann, London

DePaolo DJ (1981) Trace element and isotopic effects of combined wallrock assimilation and fractional crystallization. Earth Planet Sci Lett 53: 189–202

Deruelle B, Moreau C, Nkoumbou C, Kambou R, Lissom J, Njofang E, Ghogomu RT, Nono A (1991) The Cameroon Line: a review. In: Kampunzu AB, Lubala RT (eds) Magmatism in extensional tectonic structural settings. Springer, Berlin New York Heidelberg, pp 274–327

Dixon JE, Clague DA, Wallace P, Poreda R (1997) Volatiles in alkalic basalts from the North Arch volcanic field, Hawaii: extensive degassing of deep submarine-erupted alkalic series lavas. J Petrol 38: 911–939

Dunlop HM (1983) Strontium isotope geochemistry and potassium-argon study on volcanic rocks from the Cameroon Line, West Africa. PhD thesis, Univ. Edinburgh, UK

Fairhead JD, Okereke CS (1987) A regional study of the West African Rift system in Nigeria and Cameroon and its tectonic interpretation. Tectonophysics 143: 141–159

Fairhead JD, Okereke, CS (1990) Crustal thinning and extension beneath the Benue Trough based on gravity studies. J Afr Earth Sci 11: 329–335

Faure G (1987) Principles of isotope geology. Wiley, New York

Fitton JG (1987) The Cameroon Line, West Africa: a comparison between oceanic and continental alkaline volcanism. In: Fitton JG, Upton BGJ (eds) Alkaline igneous rocks. Geol Soc London, Spec Publ 30: 273–291

Fitton JG, Dunlop HM (1985) The Cameroon Line, West Africa and its bearing on the origin of oceanic and continental alkalic basalt. Earth Planet Sci Lett 72: 23–38

Foland KA, Landoll JD, Henderson CMB, Jianfeng C (1993) Formation of cogenetic quartz and nepheline syenites. Geochim Cosmochim Acta 57: 697–704

Ghiorso MS, Sack RO (1995) Chemical mass transfer in magmatic processes IV. A revised and internally consistent thermodynamic model for the interpolation and extrapolation of liquid-solid equilibria in magmatic systems at elevated temperatures and pressures. Contrib Mineral Petrol 119: 197–212

Gibson IL (1974) A review of the geology, petrology and geochemistry of the volcano Fantale. Bull Volc and 38: 791–802

Govindaraju K, Mevelle G (1987) Fully automated dissolution and separation methods for inductively coupled plasma atomic emission spectrometry rock analysis. Application to the determination of rare earth elements. J Anal Atom Spectr 2: 615–621

Green TH (1994) Experimental studies of trace element partitioning applicable to igneous petrogenesis – Sedona 16 years later. Chem Geol 117: 1–36

Halliday, AN, Dickin, AP, Fallick, AE, Fitton, JG (1988) Mantle dynamics: a Nd, Sr, Pb and O isotopic study of the Cameroon line volcanic chain. J Petrol 29: 181–211

Hanson GN (1978) The application of trace elements to the petrogenesis of igneous rocks of granitic composition. Earth Planet Sci Lett 38: 26–43

Hay DE, Wendlandt RF (1995) The origin of Kenya rift-type flood phonolites: results of high-pressure/high-temperature experiments in the system phonolite-H_2O and phonolite-H_2O-CO_2. J Geophys Res 100: 401–410

Iacumin P, Piccirillo EM, Longinelli A (1991) Oxygen isotopic composition of Lower Cretaceous tholeiites and Precambrian basement rocks from the Paranà basin (Brazil): the role of water-rock interaction. Chem Geol (Isotope Geosci Sect) 86: 225–237

Kampunzu AB, Lubala RT (eds) (1991) Magmatism in extensional tectonic structural settings. Springer, Berlin, New York, Heidelberg

Landoll JD, Foland KA, Henderson CMB (1994) Nd isotopes demonstrate the role of contamination in the formation of coexisting quartz and nepheline syenites at the Abu Khruq complex, Egypt. Contrib Mineral Petrol 117: 305–329

LeBas MJ, Le Maitre RW, Streckeisen A, Zanettin B (1986) Chemical classification of volcanic rocks based on the total alkali-silica diagram. J Petrol 27: 745–750

Lee DC, Halliday AN, Fitton JG, Poli G (1994a) Isotopic variations with distance and time in the volcanic islands of the Cameroon line: evidence for a mantle plume origin. Earth Planet Sci Lett 123: 119–138

Lee DC, Halliday AN, Hall CM, Fitton JG (1994b) Similarities and differences between continental and oceanic basalts in the Cameroon Line (abstract). Eighth International Conference on Geochronology, Cosmochronology and Isotope Geology, Berkeley, p 188

LeMarchand F, Villemant B, Calas G (1987) Trace element distribution coefficients in alkaline series. Geochim Cosmochim Acta 51: 1071–1081

Lowsteren JB, Mahood GA (1991) New data on magmatic H_2O contents of pantellerites, with implications for petrogenesis and eruptive dynamics at Pantelleria. Bull Volc anol 54: 78–83

Macdonald R (1974) Nomenclature and petrochemistry of the peralkaline oversaturated extrusive rocks. Bull Volcanol 35: 78–83

Macdonald R (1987) Quaternary peralkaline silicic rocks and caldera volcanoes of Kenya. In: Fitton JG, Upton BGJ (eds) Alkaline igneous rocks. Geol Soc London Spec Publ 30: 313–333

Mahood GA (1984) Pyroclastic rocks and calderas associated with strongly peralkaline magmatism. J Geophys Res 89: 8540–8552
Mahood GA, Baker DR (1986) Experimental constraints on depths of fractionation of mildly alkalic basalts and associated felsic rocks: Pantelleria, Strait of Sicily. Contrib Mineral Petrol 93: 251–264
Mahood GA, Stimac JA (1990) Trace-element partitioning in pantellerites and trachytes. Geochim Cosmochim Acta 54: 2257–2276
Marzoli A (1996) II magmatismo del settore continentale della Linea Vulcanica del Cameroon. PhD thesis, Università Trieste, Italy
Mungall JE, Martin RF (1995) Petrogenesis of basalt-comendite and basalt-pantellerite suites, Terceira, Azores, and some implications for the origin of ocean-island rhyolites. Contrib Mineral Petrol 119: 43–55
Nono A, Deruelle B, Demaiffe D, Kambouc R (1994) Tchabal Nganha volcano in Adamawa (Cameroon): petrology of continental alkaline lava series. J Volcanol Geotherm Res 60: 147–177
Panter KS, Kyle PR, Smellie JL (1997) Petrogenesis of a phonolite-trachyte succession at Mount Sidley, Marie Byrd Land, Antarctica. J Petrol 38: 1225–1253
Papike JJ, Cameron K, Baldwin K (1974) Amphiboles and pyroxenes: characterization of other than quadrilateral components and estimates of ferric iron from microprobe data. Bull Geol Soc Am 6: 1053–1054
Philips (1994) X40 software for XRF analysis. Software operational manual. Philips Bedrijven, Nederland
Plomerova J, Babuska V, Dorbath L, Lillie R (1993) Deep lithospheric structure across the Central African Shear Zone in Cameroon. Geophys J Int 115: 381–390
Pollitz FF (1991) Two stage model of African absolute motion during the last 30 million years. Tectonophysics 194: 91–106
Poudjom Djomani YH, Nnange JM, Diament M, Ebinger CJ, Fairhead JD (1995) Effective elastic thickness and crustal thickness variations in west-central Africa inferred from gravity data. J Geophys Res 100(B11): 22047–22070
Poudjom Djomani YH, Diament M, Wilson M (1997) Lithospheric structure across the Adamawa plateau (Cameroon) from gravity studies. Tectonophysics 273: 317–327
Renne PR (1995) Excess ^{40}Ar in biotite and hornblende from the Noril'sk 1 intrusion, Siberia: implications for the age of the Siberian Traps. Earth Planet Sci Lett 131: 165–176
Salviulo G, Secco L, Marzoli A, Piccirillo EM, Nyobe JB (1998) Ca-rich pyroxene from basic and silicic volcanics from the Cameroon Volcanic Line (W-Africa): crystal chemistry and petrological implications. Mineral Petrol: submitted
Silver PG, Russo RM, Lithgow-Bertelloni C (1998) Coupling of South American and African plate motion and plate deformation. Science 279: 60–63
Stormer JC, Nicholls J (1978) XLFRAC: a program for interactive testing of magmatic differentiation models. Computers and Geosciences 4: 143–159
Thy P, Lofgren GE (1992) Experimental constraints on the low pressure evolution of transitional and mildly alkalic basalts: multisaturated liquids and coexisting augites. Contrib Mineral Petrol 112: 196–202
Wilding MC, Macdonald R, Davies JE, Fallick AE (1993) Volatile characteristics of peralkaline rhyolites from Kenya: an ion microprobe, infrared spectroscopic and hydrogen isotope study. Contrib Mineral Petrol 114: 264–275
Wilson M, Downes H, Cebria JM (1995) Contrasting fractionation trends in coexisting continental alkaline magma series; Cantal, Massif Central, France. J Petrol 36: 1729–1753